OFDM-Based Novel Waveform Design for 5G and Beyond Wireless Communication Networks

by

Ali Tuğberk Doğukan

A Dissertation Submitted to the
Graduate School of Sciences and Engineering
in Partial Fulfillment of the Requirements for
the Degree of

Master of Science

in

Electrical and Electronics Engineering

KOÇ ÜNİVERSİTESİ

July 15, 2020

OFDM-Based Novel Waveform Design for 5G and Beyond Wireless Communication Networks

Koç University
Graduate School of Sciences and Engineering
This is to certify that I have examined this copy of a master's thesis by

Ali Tuğberk Doğukan

and have found that it is complete and satisfactory in all respects,
and that any and all revisions required by the final
examining committee have been made.

Committee Members:

Assoc. Prof. Ertuğrul Başar (Advisor)

Prof. Sinem Çöleri

Prof. Hüseyin Arslan

Date: ______________________

To my dear family,

ABSTRACT

OFDM-Based Novel Waveform Design for 5G and Beyond Wireless Communication Networks
Ali Tuğberk Doğukan
Master of Science in Electrical and Electronics Engineering
July 15, 2020

Orthogonal frequency division multiplexing (OFDM) with index modulation (OFDM-IM) appears as a promising multi-carrier waveform candidate for 5G and beyond wireless networks due to its attractive advantages such as superior error performance, operational flexibility, and ease of implementation. OFDM-IM itself may not be a proper choice for 5G services such as enhanced mobile broadband (eMBB) and ultra-reliable and low-latency communications (URLLC) since achieving high data rates is challenging because of its null subcarriers and also its error performance is not at a sufficient level for mission critical applications. However, the flexible structure of OFDM-IM has a great potential and more sophisticated OFDM-IM-based waveforms can be designed to meet the requirements of future eMBB and URLLC applications. For eMBB, one solution to enhance the spectral efficiency of OFDM-IM is the employment of multiple distinguishable constellations (modes) by also exploiting its null subcarriers for data transmission. Furthermore, an OFDM-IM block with a sparse structure can be utilized to generate a suitable waveform for URLLC applications. In this thesis, application-based novel waveforms are designed by enjoying the appealing features of OFDM-IM.

In Chapter 1, a novel IM technique called super-mode OFDM-IM (SuM-OFDM-IM) is proposed, where mode activation patterns (MAPs) and subcarrier activation patterns (SAPs) are jointly selected and conventional data symbols are repetition coded over multiple subcarriers to achieve a diversity gain. For the proposed scheme, a low-complexity detector is designed, theoretical analyses are performed and a bit error rate (BER) upper bound is derived. The performance of the proposed system is also investigated through real-time experiments using a software-defined radio (SDR) based prototype. It is shown that SuM-OFDM-IM exhibits promising results in terms of spectral efficiency and error performance; thus, appears as a potential

candidate for 5G and beyond communication systems.

In Chapter 2, OFDM with power distribution index modulation (OFDM-PIM) is proposed where a unique power distribution technique is applied to index modulated subcarriers. Furthermore, OFDM with in-phase/quadrature PIM (OFDM-I/Q-PIM), which independently performs the same power distribution process on the real and imaginary parts of the data symbols, is proposed. Average bit error probabilities (ABEP) of OFDM-PIM and OFDM-I/Q-PIM are obtained and the superiority of the proposed schemes over reference schemes is demonstrated via extensive computer simulations.

Finally, in Chapter 3, a low-complexity encoding/decoding algorithm is proposed for the sparse vector coding (SVC) scheme, which allows the use of all possible activation patterns (APs) without the need for a look-up table. Computer simulation results reveal that the proposed low-complexity algorithm provides not only a superior BER performance but also improved spectral efficiency compared to the ordinary SVC approach.

ÖZETÇE

5G ve Ötesi Kablosuz İletişim Ağları için OFDM Tabanlı Özgün Dalga Formu Tasarımı

Ali Tuğberk Doğukan
Elektrik ve Elektronik Mühendisliği, Yüksek Lisans
15 Temmuz 2020

İndis modülasyonlu dik frekans bölmeli çoğullama (orthogonal frequency division multiplexing with index modulation, OFDM-IM), üstün hata performansı, çalışma esnekliği ve uygulanma kolaylığı gibi cazip avantajları nedeniyle 5G ve ötesi kablosuz ağları için umut verici çok taşıyıcılı dalga formu adayı olarak ortaya çıkmaktadır. OFDM-IM'in kendisi, gelişmiş mobil geniş bant (enhanced mobile broadband, eMBB) ve aşırı güvenilir ve düşük gecikmeli haberleşme (ultra-reliable and low-latency communications, URLLC) gibi 5G hizmetleri için uygun bir seçim olmayabilir, çünkü boş alt taşıyıcıları sebebiyle yüksek veri hızlarına ulaşmak zorlayıcıdır ve kritik görev uygulamaları için de hata performansı yeterli seviyede değildir. Fakat, OFDM-IM'in esnek yapısı büyük bir potansiyele sahiptir ve gelecek eMBB ve URLLC uygulamalarının gereksinimlerini karşılamak için daha gelişmiş OFDM-IM tabanlı dalga formları tasarlanabilir. eMBB için, OFDM-IM'in bant verimliliğini arttırmak için bir çözüm, veri iletimi için boş alt taşıyıcılardan da faydalanılarak birden fazla ayırt edilebilir sinyal kümelerinin kullanılmasıdır. Ayrıca, URLLC uygulamaları için uygun bir dalga formu oluşturmak için seyrek yapılı bir OFDM-IM bloğu kullanılabilir. Bu tezde, OFDM-IM'in ilgi çekici özelliklerinden istifade edilerek, uygulama tabanlı yeni dalga formları tasarlanmıştır.

Bölüm 1'de, süper mod OFDM-IM (super-mode OFDM-IM, SuM-OFDM-IM) adı verilen özgün bir IM tekniği önerilmektedir, burada mod etkinleştirme paternleri (mode activation patterns, MAPs) ve alt taşıyıcı etkinleştirme paternleri (subcarrier activation patterns, SAPs) birlikte seçilmekte ve geleneksel veri sembolleri birden fazla alt taşıyıcı üzerinde çeşitleme kazancı sağlamak amacıyla tekrardan kodlanmaktadır. Önerilen şema için, düşük karmaşıklıkta bir alıcı tasarlandı, teorik analizler gerçekleştirildi ve bit hata oranı (bit error rate, BER) üst sınırı elde edildi. Önerilen sistemin performansı, yazılım tabanlı radyo (software-defined radio, SDR)

tabanlı bir prototip kullanılarak yapılan gerçek zamanlı deneylerle de incelenmektedir. SuM-OFDM-IM'in bant verimliliği ve hata performansı açısından ümit verici sonuçlar sergilediği gösterilmekte; bu nedenle, 5G ve ötesi haberleşme sistemleri için potansiyel bir aday olarak görülmektedir.

Bölüm 2'de, indis modülasyonlu alt taşıyıcılara özgün bir güç dağıtım tekniğinin uygulandığı güç dağıtım indis modülasyonlu OFDM (OFDM with power distribution index modulation, OFDM-PIM) şeması önerilmektedir. Ayrıca, veri sembollerinin gerçek ve sanal kısımlarında bağımsız olarak aynı güç dağıtım işleminin uygulandığı fazda/dik PIM'li OFDM (OFDM with in-phase/quadrature PIM, OFDM-I/Q-PIM) şeması önerilmektedir. OFDM-PIM ve OFDM-I/Q-PIM şemalarının ortalama bit hata olasılıkları (average bit error probability, ABEP) elde edilmekte ve önerilen şemaların referans şemalara göre üstünlükleri kapsamlı bilgisayar benzetimleri ile gösterilmektedir.

Son olarak, Bölüm 3'te, seyrek vektör kodlama (sparse vector coding, SVC) şeması için bir arama tablosuna ihtiyaç duymadan tüm olası etkinleştirme paternlerini (activation pattern, AP) kullanabilen düşük karmaşıklıklı bir kodlama/kod çözme algoritması önerilmektedir. Bilgisayar benzetim sonuçları, önerilen düşük karmaşıklıklı algoritmanın sadece üstün bir BER performansı sağlamakla kalmayıp, aynı zamanda sıradan SVC yaklaşımına kıyasla arttırılmış bant verimliliği sağladığını göstermektedir.

ACKNOWLEDGMENTS

First, I would like to thank my dear advisor Dr. Ertuğrul Başar for always supporting, motivating and believing in me ever since I met him. He has not only guided us to improve academically but also taught us life lessons such as time management and organization. Second, I would also like to acknowledge my lovely mother Mürüvvet, dear father Ayhan, and full of life brothers Tuğşad, Ceyhun and Orhun for their continuous love, support and trust. Finally, I would like to thank my friend Emre Arslan who is like a brother to me and my beloved Serranur Tümer for always being by my side and pushing me to be my best.

TABLE OF CONTENTS

LIST OF TABLES

LIST OF FIGURES

ABBREVIATIONS

ABEP	Average Bit Error Probability
AP	Activation Pattern
BER	Bit Error Rate
CC	Convolutional Coding
CFO	Carrier Frequency Offset
CIR	Channel Impulse Response
CM	Complex Multiplication
CP	Cyclic Prefix
CPEP	Conditional Pairwise Error Probability
CS	Compressed Sensing
eMBB	Enhanced Mobile Broadband
FFT	Fast Fourier Transform
IEEE	The Institute of Electrical and Electronics Engineers
IET	Institution of Engineering and Technology
IFFT	Inverse Fast Fourier Transform
IM	Index Modulation
IoT	Internet of Things
LLR	Log-Likelihood Ratio
LTE	Long-Term Evolution
MAP	Mode Activation Pattern
MIAD	Minimum Intra-Mode Distance
MIMO	Multiple-Input Multiple-Output
MIRD	Minimum Inter-Mode Distance
ML	Maximum Likelihood
MMP-DF	Multipath Matching Pursuit With Depth-First

mMTC	Massive Machine-Type Communications
OFDM	Orthogonal Frequency Division Multiplexing
QAM	Quadrature Amplitude Modulation
PEP	Pairwise Error Probability
PSK	Phase Shift Keying
RF	Radio Frequency
SAP	Subcarrier Activation Pattern
SDR	Software Defined Radio
SM	Spatial Modulation
SNR	Signal-to-Noise Ratio
SSK	Space Shift Keying
SVC	Sparse Vector Coding
TO	Timing Offset
TVT	Transactions on Vehicular Technology
TWC	Transactions on Wireless Communications
UPEP	Unconditional Pairwise Error Probability
URLLC	Ultra-Reliable and Low-Latency Communications
USRP	Universal Software Radio Peripheral
VDD	Virtual Digital Domain
VI	Virtual Instrument

Chapter 1

INTRODUCTION

Wireless communication technologies play an important role in today's modern world. Secure data transmission and reception over a wireless link are crucial for the sustainability of our daily lives. As the developments in science and technology progress day by day, the need for more sophisticated and innovative wireless communication solutions increases. The aforementioned developments led to the emergence of wireless communication applications with different requirements. These applications are supported by 5G wireless systems via three main services: ultra-reliable and low-latency communications (URLLC), massive machine-type communications (mMTC), and enhanced mobile broadband (eMBB) [Popovski et al., 2018]. These services can be briefly explained as follows: (a) URLLC supports reliable and low-latency communication with low data rate, (b) mMTC supports the connection of a very large number of Internet of Things (IoT) devices, (c) eMBB provides high data rate over a wide coverage area. For these services to be applicable in the practical life, specific waveforms should be designed by taking into consideration completely different requirements and demands of these services. Waveform is one of the core components of the physical layer design and determines the time-frequency utilization of the transmitted signal.

Orthogonal frequency division multiplexing (OFDM) is a very popular multi-carrier transmission system which has been used in many standards such as IEEE 802.11x and Long Term Evolution (LTE). Even though OFDM is not relatively new, it still maintains its importance for state-of-the-art wireless communication technologies due to its simple and easily implementable structure. OFDM is the selected waveform for 5G wireless networks thanks to its several advantages such as simplicity, multiple-input multiple-output (MIMO) and backward compability, and robustness to frequency selective fading. In the literature, numerous studies have been done by researchers to enhance the performance of OFDM. A very simple diversity-enhancing scheme called repetition coded OFDM (RC-OFDM) [Sasamori et al., 2011] is proposed where repetition coding is applied to OFDM subcarriers to improve its error performance. However, it is difficult to achieve high spectral efficiencies with RC-OFDM since it exploits multiple subcarriers (frequency resources) for the transmission of the same data symbol.

Index modulation (IM) [Basar, 2016a], which employs the indices of transmit entities such as antennas, time slots, and radio frequency (RF) mirrors, has attracted significant attention from the researchers due to its advantages over conventional communication systems in terms of transceiver complexity and spectral/energy efficiency. These attractive features of IM make it a potential candidate for communication systems beyond 5G. IM has been employed in numerous dimensions as mentioned above, and it can also be implemented in the frequency domain by utilizing the indices of the available subcarriers of multi-carrier systems [Basar et al., 2017, Mao et al., 2018]. In [Basar et al., 2013a], OFDM has been effectively combined with IM by activating a number of subcarriers in a subblock while de-activating the remaining ones.

In this thesis, by employing the flexibility of IM, three novel OFDM-based and application-oriented waveforms are designed for different 5G services (eMBB and URLLC).

1.1 Contributions

In this thesis, firstly, a novel OFDM-based transmission system called *super-mode OFDM-IM (SuM-OFDM-IM)*, which is capable of yielding both a diversity gain and a high spectral efficiency, is proposed. In SuM-OFDM-IM, according to the incoming bits, mode activation patterns (MAPs) and subcarrier activation patterns (SAPs) are jointly determined; therefore, additional information bits can be transmitted by IM. The determination of MAPs and SAPs separately is also considered to provide an alternative solution and this scheme is called *separated SuM-OFDM-IM (S-SuM-OFDM-IM)*. It is well known that the bits transmitted by IM are more reliable than the ones transmitted by conventional Q-ary PSK/QAM. In other words, conventional PSK/QAM symbols restrict the diversity gain of the system. In our scheme, repetition coding is applied to the modulated symbols drawn from the selected modes over multiple subcarriers to attain a diversity gain. A novel encoding technique is proposed as well as a log-likelihood ratio (LLR)-based reduced complexity maximum likelihood (ML) detection algorithm. Additionally, real-time error performance of the proposed system is investigated through a practical testbed at Koç University-CoreLab using software-defined radio (SDR) units.

Secondly, *OFDM with power distribution index modulation (OFDM-PIM)* is proposed where information bits are transmitted by both conventional data symbols and subcarrier indices along with high/low power levels. In OFDM-PIM, each data symbol is distributed over two subcarriers with high/low power levels. To further increase the number of bits conveyed by IM, *OFDM with in-phase/quadrature PIM (OFDM-I/Q-PIM)*, which extends OFDM-PIM to in-phase and quadrature dimensions, is proposed. In OFDM-I/Q-PIM, the subcarrier indices for high/low power levels are determined twice for both real and imaginary parts of the data symbols. The derivation of the average bit error probability (ABEP) and the power level selection strategy are given for OFDM-PIM and OFDM-I/Q-PIM. It is revealed via computer simulations that OFDM-PIM and OFDM-I/Q-PIM outperform their counterparts.

Finally, a clever encoding/decoding technique is proposed for SVC-OFDM, which is referred to as *enhanced SVC-OFDM (E-SVC-OFDM)*. E-SVC-OFDM increases the number of bits transmitted by IM in an intelligent manner. The multipath matching pursuit with depth-first (MMP-DF) algorithm is used for detection and since the sparsity of the system is high, it can be considered as a system with low complexity as in [Kwon et al., 2014]. SVC-OFDM exploits a certain number of possible activation patterns (APs) of the active indices and provides multiple sparse vectors to use for data transmission. However, it is not always possible to use all possible APs since the total number of combinations is not an integer power of two.

To solve this problem, E-SVC-OFDM runs a clever algorithm that allows the use of all possible APs, hence, the number of bits transmitted by APs is also increased.

The contributions of this thesis are published as three journal papers. SuM-OFDM-IM has been published in Institute of Electrical and Electronics Engineers (IEEE) Transactions on Wireless Communications (TWC). OFDM-PIM has been published in Institution of Engineering and Technology (IET) Electronics Letters. E-SVC-OFDM has been published in IEEE Transactions on Vehicular Technology (TVT).

Notation: Bold, lowercase and capital letters are exploited for column vectors and matrices, respectively. $(\cdot)^{\mathrm{T}}$, $(\cdot)^{\mathrm{H}}$, $||\cdot||$ and $||\cdot||_F$ denote transposition, Hermitian transposition, Euclidean norm, and Frobenius norm, respectively. $\mathrm{diag}(\cdot)$ and $\lfloor\cdot\rfloor$ represent diagonalization and floor operations, respectively. $\det(\mathbf{X})$ and $\mathrm{rank}(\mathbf{X})$ respectively stand for the determinant and rank of $\mathbf{X}$. $\binom{\cdot}{\cdot}$ is the binomial coefficient. $\Re\{\mathbf{x}\}$ and $\Im\{\mathbf{x}\}$ denote the real and imaginary part of complex vector $\mathbf{x}$, respectively. $\mathcal{CN}(m_x, \sigma_x^2)$ represents Gaussian distribution with mean m_x and variance σ_x^2.

Chapter 2

ORTHOGONAL FREQUENCY DIVISION MULTIPLEXING WITH INDEX MODULATION

Spatial modulation (SM) [Mesleh et al., 2006], which employs the indices of transmit antennas to transmit information, has been presented as a flexible and efficient MIMO transmission scheme. SM has been regarded as a potential transmission technique due to its various advantages such as low-complex and simple structure compared to conventional MIMO systems. Inspired by SM, OFDM-IM has been proposed by applying IM to the subcarriers of OFDM in a clever way to improve the error performance, spectral, and energy efficiency of conventional OFDM [Basar et al., 2013a].

In OFDM-IM, information bits are conveyed by not only Q-ary modulated symbols but also active subcarrier indices. Compared to conventional OFDM, it is shown that OFDM-IM is capable of providing a better error performance while consuming less power due to its null subcarriers.

2.1 Working Principle of OFDM-IM

OFDM-IM is an OFDM-based multicarrier transmission system with N subcarriers whose transmitter structure is given in Figure 2.1. As seen from Figure 2.1, a total number of m bits enter the system. These bits are separated into $g = m/p$ groups, where p is the number of bits per each group. Each group of p bits forms an OFDM subblock whose lenght is n, where $n = N/g$. To create αth subblock $\mathbf{s}_\alpha$, these p bits are split into two parts:

1. $p_1 = \lfloor \log_2 \binom{n}{k} \rfloor$

2. $p_2 = k \log_2(Q)$

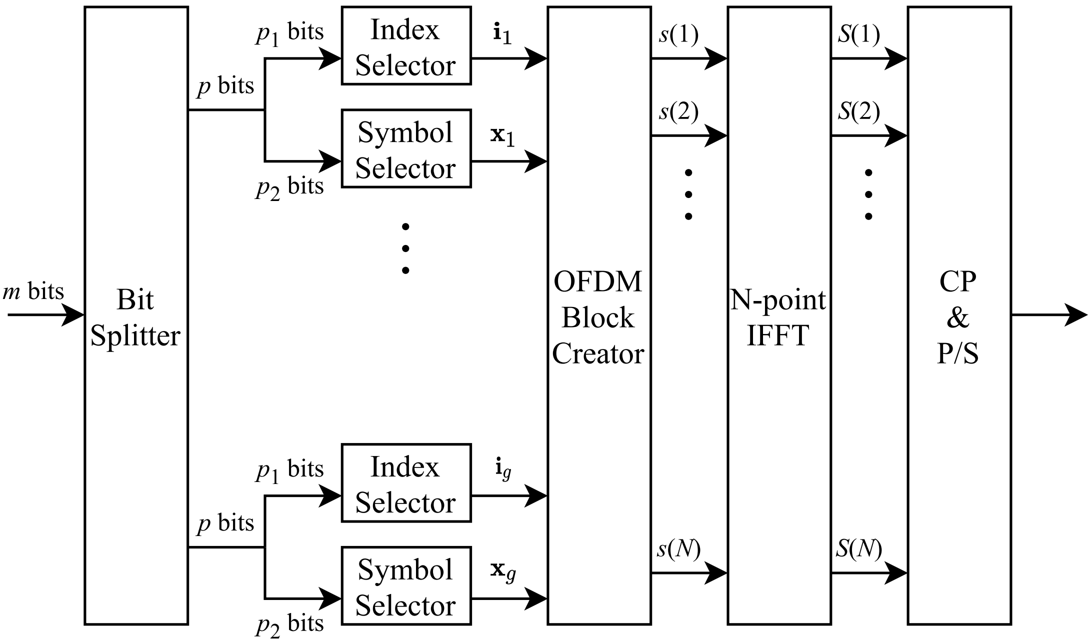

Figure 2.1: Transmitter Structure of OFDM-IM.

where Q and k are the modulation order and the number of active indices in a sub-block, respectively. Firstly, p_1 bits determine the active indices $\mathbf{i}_\alpha = [i_\alpha(1), \cdots, i_\alpha(k)]$, $i_\alpha(\xi) \in \{1, \cdots, n\}$, $\xi = 1, \cdots, k$. Secondly, p_2 bits determine the modulated symbols $\mathbf{x}_\alpha = [x_\alpha(1), \cdots, x_\alpha(k)]$, $x_\alpha(\xi) \in \mathcal{X}$, where $\mathcal{X}$ represents the Q-QAM/PSK signal constellation and is normalized to unity. By taking into consideration $\mathbf{i}_\alpha$ and $\mathbf{x}_\alpha$, $\mathbf{s}_\alpha$ is created. Same procedures are applied for each subblock and overall OFDM block $\mathbf{s} = [\mathbf{s}_1^{\mathrm{T}}\mathbf{s}_2^{\mathrm{T}} \cdots \mathbf{s}_G^{\mathrm{T}}]^{\mathrm{T}} = [s(1) \cdots s(N)]^{\mathrm{T}}$ is obtained. Inverse fast Fourier transform (IFFT) is performed to obtain time-domain OFDM block. Then, a cyclic prefix (CP) of length C_p is added, parallel-to-serial, and digital-to-analog conversions are performed. The signal is transmitted over a T-tap frequency-selective Rayleigh fading channel whose elements follow $\mathcal{CN}(0, \frac{1}{T})$ distribution. During the transmission of OFDM signal, it is assumed that the channel remains constant and C_p is greater than T. Consequently, the equivalent frequency domain relationship is obtained as:

$$y(\gamma) = h(\gamma)s(\gamma) + w(\gamma), \;\; \gamma = 1, \cdots, N, \tag{2.1}$$

where $y(\gamma)$, $h(\gamma)$, and $w(\gamma)$ are the received signals, channel fading coefficients, and the noise samples in the frequency domain. The distributions of $h(\gamma)$ and

$w(\gamma)$ are given as $\mathcal{CN}(0,1)$ and $\mathcal{CN}(0,N_{0,F})$, respectively, where $N_{0,F}$ is the noise variance in the frequecny domain. The noise variance in the time domain is given as $N_{0,T} = (\frac{n}{k})N_{0,F}$.

Received signal and channel coefficients vectors corresponding to αth subblock are represented as $\mathbf{y}_\alpha = [y(\alpha n-(n-1)), \cdots, y(\alpha n))]^{\mathrm{T}}$ and $\mathbf{h}_\alpha = [h(\alpha n-(n-1)), \cdots, h(\alpha n))]^{\mathrm{T}}$, respectively. The ML detector can be used to decode the αth subblock by employing the set $\mathcal{Z} \in \{\mathbf{z}_1, \cdots, \mathbf{z}_{2^p}\}$ which contains all possible subblock realizations:

$$\hat{\mathbf{s}}_\alpha = \arg\min_{\mathbf{z}\in\mathcal{Z}} \|\mathbf{y}_\alpha - \mathbf{Z}\mathbf{h}_\alpha\|^2, \tag{2.2}$$

where $\mathbf{Z} = \mathrm{diag}(\mathbf{z}) \in \mathbb{C}^{n\times n}$.

It is shown that OFDM-IM provides significant gains over conventional OFDM in terms of error performance [Basar et al., 2013a]. Due to its highly flexible structure, many studies have been done by researchers to further improve the performance of OFDM-IM. These are briefly discussed in the following section.

2.2 A Brief Literature Survey on OFDM-IM

OFDM-IM has attracted significant interest from researchers due to its highly flexible architecture. The error performance of OFDM-IM is improved by employing a subcarrier-level block interleaver [Xiao et al., 2014]. To further enhance the error performance of OFDM-IM, coordinate interleaved OFDM-IM (CI-OFDM-IM), which provides a diversity gain by transmitting the real and imaginary parts of modulated symbols over different active subcarriers, is proposed in [Basar, 2015]. In [Jaradat et al., 2018], OFDM with subcarrier number modulation (OFDM-SNM) is proposed where the number of active subcarriers in a subblock is determined by the incoming bits. A clever technique that decreases the modulation order while increasing the number of bits transmitted by IM without any reduction in spectral efficiency, is proposed [Nambi and Giridhar, 2018]. An energy- and spectrum-efficient system that employs unused subcarrier activation patterns (SAPs) in OFDM-IM by selecting a certain number of adjacent subblocks jointly, is proposed in [Shi et al., 2019]. In recent years, OFDM-IM has also been applied to emerging communication systems such as dual-hop networks [Dang et al., 2018b, Dang et al., 2018a], multiple-input multiple-output (MIMO) systems [Basar, 2016b, Zheng et al., 2017, Öztürk et al., 2019, Lu et al., 2018], cognitive radio [Ma et al., 2017, Li et al., 2019] and optical communications [Başar and Panayırcı, 2015]. By using nonzero elements in OFDM-IM transmission block, sparse vector coding (SVC) is applied to OFDM-IM and a novel OFDM-based waveform is proposed for URLLC applications [Ji et al., 2018].

Because of its null subcarriers, achieving very high data rates with OFDM-IM is not possible and this may be critical for future eMBB applications such as augmented/virtual reality (AR/VR) and 4K/8K video streaming. To overcome this critical drawback, multiple constellations are utilized by activating not only the selected subcarriers but also the null ones. Dual-mode aided OFDM (DM-OFDM), which also utilizes the null subcarriers to transmit data symbols drawn from a secondary distinguishable constellation, is proposed in [Mao et al., 2017b]. In [Zheng and Chen, 2017], a diversity gain is achieved by transmitting the same data symbols through re-activation of the null subcarriers with a second mode. DM-OFDM is generalized in [Mao et al., 2017a] by changing the number of subcarriers drawn from the same constellation. The performance of DM-OFDM and OFDM-IM has been investigated in real-time by adopting software defined radios (SDRs) in [Gokceli et al., 2017]. In DM-OFDM, only two different constellations are considered; however, multiple-mode OFDM-IM (MM-OFDM-IM), which exploits all n subcarriers in each subblock with n different distinguishable modes, is proposed to employ more number of constellations [Wen et al., 2017]. MM-OFDM-IM uses the full permutations of these constellations to apply IM. In [Wen et al., 2018], a generalized version of MM-OFDM-IM is proposed where the size of the constellations can be altered although there is no increase in the number of bits conveyed by IM. To obtain diversity gains, coordinate interleaved MM-OFDM-IM (CI-MM-OFDM-IM) and linear constellation precoded MM-OFDM-IM (LCP-MM-OFDM-IM) schemes have been presented [Li et al., 2018]. Although these noticeable improvements, there is still an undeniable need for multi-carrier waveforms that provide reliable error performance and high data rate for future URLLC and eMBB services, respectively.

Chapter 3

SUPER-MODE OFDM WITH INDEX MODULATION

It is well-known that OFDM-IM provides several advantages compared to OFDM; neverthless, its error performance and spectral efficiency are not satisfactory for future eMBB applications. Thus, a more sophisticated waveform, which enhances the performance of OFDM-IM, should be designed.

SuM-OFDM-IM is a novel OFDM-based transmission system that provides a diversity gain, superior error performance, and high spectral efficiency. In this scheme, MAPs and SAPs are jointly selected to increase the number of bits conveyed by IM. Additionally, repetition coding is applied to data symbols over multiple subcarriers to provide diversity for them as well. Due to its higher diversity order and smart encoding technique, SuM-OFDM-IM provides considerable gain over OFDM-IM and OFDM-IM-based schemes.

In this chapter, the system model, performance analysis, simulation results, and experimental results of SuM-OFDM-IM are given.

3.1 System Model of SuM-OFDM-IM

In this section, firstly, an encoding algorithm is introduced for SuM-OFDM-IM, which jointly determines MAP and SAP in order to increase the number of bits conveyed by IM. A clever symbol assignment strategy is also considered to provide a diversity gain. Second, a novel LLR-based reduced complexity ML detector is proposed.

3.1.1 Transmitter

SuM-OFDM-IM is an OFDM-based transmission system with N subcarriers whose transmitter structure is given in Figure 3.1. A total of m bits are conveyed for

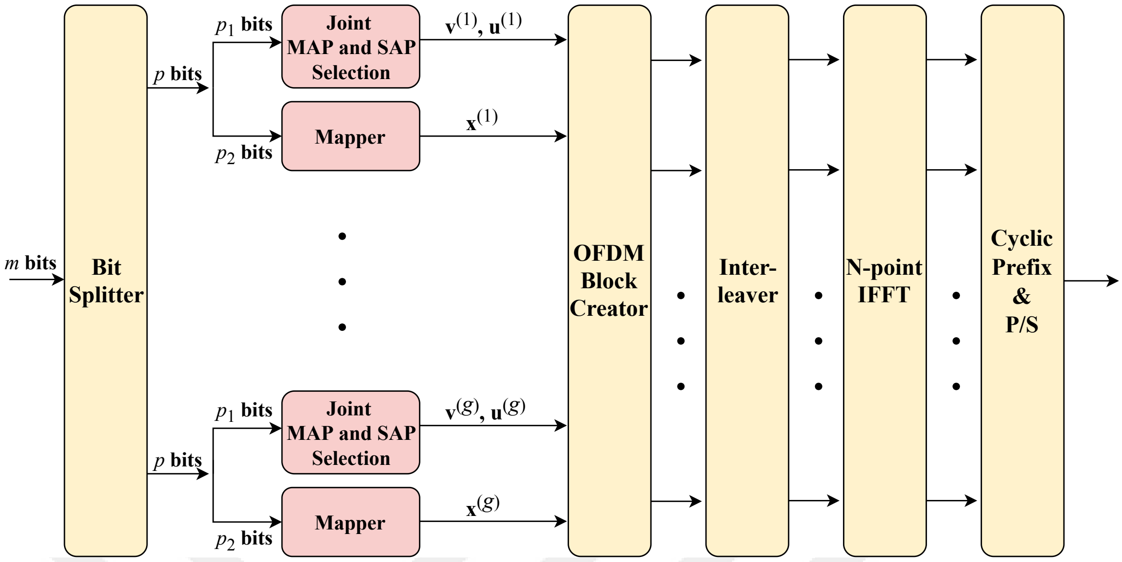

Figure 3.1: Transmitter Structure of SuM-OFDM-IM.

each symbol transmission and split into groups with $p = m/g$ bits, where g is the number of subblocks. Since the same procedures are applied for each subblock, for convenience, the mapping of p bits into the αth subblock $\mathbf{s}^{(\alpha)}$, is considered, where $\alpha \in \{1, \dots, g\}$. These p bits are split into two parts:

1. $p_1 = \lfloor \log_2(\binom{M}{2}\binom{n}{n/2}) \rfloor$

2. $p_2 = \frac{n}{2} \log_2 Q$

where n, M and Q are the size of the subblock, $n = 2^r, r \in \{2, 3, \dots\}$, the total number of modes, and constellation size, respectively. First, p_1 bits jointly determine an MAP ($\mathbf{v}^{(\alpha)} = [v_1, v_2], v_l \in \{1, \dots, M\}, l = 1, 2$) and an SAP ($\mathbf{u}^{(\alpha)} = [u_1, \dots, u_{n/2}], u_m \in \{1, \dots, n\}, m = 1, \dots, n/2$), where this joint selection is discussed in the sequel. Here, the selected MAP includes two different modes to be able to employ IM ($v_1 \neq v_2$) and the strategy for mode selection is discussed in Section 3.2. We also activate $n/2$ subcarriers per mode to maximize p_1. The remaining indices that are not included in a selected SAP are represented by $\mathbf{w}^{(\alpha)} = [u_{n/2+1}, \dots, u_n]$. The subcarrier indices $\mathbf{u}^{(\alpha)}$ and $\mathbf{w}^{(\alpha)}$ are exploited for the symbols drawn from the first and second modes, respectively. Then, since each symbol is repetition coded over a pair of subcarriers, $\mathbf{u}^{(\alpha)}$ and $\mathbf{w}^{(\alpha)}$ are split into $n/4$

groups ($\mathbf{u}_k^{(\alpha)} = [u_{2k-1}, u_{2k}], \mathbf{w}_k^{(\alpha)} = [u_{n/2+2k-1}, u_{n/2+2k}], k = 1, \ldots, n/4$. Second, $\frac{p_2}{2} = \frac{n}{4}\log_2 Q$ bits determine the first $n/4$ modulated symbols ($\mathbf{x}_1^{(\alpha)} = [x_1, \ldots, x_{n/4}]$), which are drawn from $\mathcal{M}_{v_1}$, $\mathcal{M}_i = \{\chi_{i1}, \ldots, \chi_{iQ}\}, i \in \{1, \ldots, M\}$, where χ_{iq} is the qth symbol of the ith mode and the set of all modes is $\mathcal{M} = \{\mathcal{M}_1, \ldots, \mathcal{M}_M\}$. The average symbol power of $\mathcal{M}$ is normalized to unity. Finally, $\frac{p_2}{2} = \frac{n}{4}\log_2 Q$ bits determine the last $n/4$ modulated symbols ($\mathbf{x}_2^{(\alpha)} = [x_{n/4+1}, \ldots, x_{n/2}]$), which are drawn from $\mathcal{M}_{v_2}$, and we obtain $\mathbf{x}^{(\alpha)} = [\mathbf{x}_1^{(\alpha)}\mathbf{x}_2^{(\alpha)}]$. The kth element of $\mathbf{x}_1^{(\alpha)}$ and $\mathbf{x}_2^{(\alpha)}$ are repetition coded over the subcarriers of the target subblock with the indices given by $\mathbf{u}_k^{(\alpha)}$ and $\mathbf{w}_k^{(\alpha)}$, respectively. By performing the same steps for all elements of $\mathbf{x}_1^{(\alpha)}$ and $\mathbf{x}_2^{(\alpha)}$, $\mathbf{s}^{(\alpha)}$ is created. Consequently, a total of

$$p = \left\lfloor \log_2 \left(\binom{M}{2} \binom{n}{n/2} \right) \right\rfloor + \frac{n}{2}\log_2 Q \tag{3.1}$$

bits are transmitted per subblock.

The aim of this joint MAP and SAP selection is to further increase the number of bits conveyed by IM. The proposed joint selection algorithm of MAP and SAP is summarized below:

1. Convert p_1 bits to a decimal number: d.

2. Find the unique values (a_1, a_2) satisfying the equation:

   $$d = a_1 + \binom{M}{2} a_2, \tag{3.2}$$

   where $a_1 \in \{0, \ldots, \binom{M}{2} - 1\}$ and $a_2 \in \{0, \ldots, \binom{n}{n/2} - 1\}$ are the indices of the selected MAP and SAP, respectively.

3. Determine MAP ($\mathbf{v}^{(\alpha)}$) and SAP ($\mathbf{u}^{(\alpha)}$) by applying a_1 and a_2 to the combinatorial algorithm [Basar et al., 2013a], respectively.

Example: Assuming $M = 4, n = 4, Q = 4$, the number of bits conveyed by IM is $p_1 = \lfloor \log_2(\binom{4}{2}\binom{4}{4/2}) \rfloor = 5$ and the number of bits conveyed by conventional data symbols is $p_2 = \frac{4}{2}\log_2(4) = 4$. For this case, a total of $\binom{4}{2} = 6$ MAPs and $\binom{4}{2} = 6$ SAPs are obtained as in Table 3.1 There are 36 possible pairs of (a_1, a_2) and 32 of

Table 3.1: Joint Selection of MAP and SAP

a_1	$[v_1, v_2]$	a_2	$[u_1, u_2]$
0	$[1,2]$	0	$[1,2]$
1	$[1,3]$	1	$[1,3]$
2	$[2,3]$	2	$[2,3]$
3	$[1,4]$	3	$[1,4]$
4	$[2,4]$	4	$[2,4]$
5	$[3,4]$	5	$[3,4]$

these are employed to transmit $\lfloor \log_2(36) \rfloor = 5$ bits. Let p_1 and p_2 be $\{01001\}$ and $\{1110\}$, respectively. The (a_1, a_2) values satisfying (2) are $(3, 2)$. In the absence of joint selection, only four bits can be transmitted per subblock instead of five by the indices of modes and subcarriers for these given parameters. Therefore, an additional bit can be conveyed by the joint selection in this specific case. Then, MAP is determined as $\mathbf{v} = [1, 4]$, i.e, $\mathcal{M}_1$ and $\mathcal{M}_4$ are employed. SAP is determined as $\mathbf{u} = [1, 3]$, so the remaining indices are $\mathbf{w} = [2, 4]$. For simplicity, we have removed the superscript (α). The first two bits of p_2, which are $\{11\}$, select the fourth symbol of the first selected mode (χ_{14}) and the second two bits of p_2, which are $\{10\}$, select the second symbol of the second selected mode (χ_{42}). Finally, χ_{14} and χ_{42} are placed into the indices of subblock entries with $\mathbf{u}$ and $\mathbf{w}$, respectively and the overall subblock is obtained as:

$$\mathbf{s} = [\chi_{14}\ \chi_{42}\ \chi_{14}\ \chi_{42}]^{\mathrm{T}}. \tag{3.3}$$

Having constructed the OFDM symbol subblock by subblock, a block-type interleaver is executed as in [Wen et al., 2017] and the same procedures applied in OFDM are performed. The inverse fast fourier transform (IFFT) algorithm is applied to the OFDM block to obtain the time domain OFDM block as:

$$\mathbf{s}_T = \mathrm{IFFT}\{\mathbf{s}_F\} = \Big[S(1)\ \ S(2)\ \ \cdots\ \ S(N)\Big]^{\mathrm{T}}. \tag{3.4}$$

Then, a cyclic prefix (CP) of length L samples $\Big[S(N-L+1)\ \cdots\ S(N-1)S(N)\Big]^{\mathrm{T}}$ is added to the beginning of the OFDM block. After parallel to serial (P/S) and digital/analog conversions are applied, the signal is transmitted over a frequency-selective Rayleigh fading channel with the channel impulse response (CIR) coefficients

$$\mathbf{c}_T = \begin{bmatrix} c_T(1) & \cdots & c_T(v) \end{bmatrix}^{\mathrm{T}}, \tag{3.5}$$

where $c_T(\beta), \beta = 1, \ldots, v$ are circularly symmetric complex Gaussian random variables with the $\mathcal{CN}(0, \frac{1}{v})$ distribution. With the assumption that the channel remains constant during transmission of an OFDM block and the CP length L is larger than v, the equivalent frequency domain input-output relationship of this OFDM scheme is given by

$$y_F(\beta) = s_F(\beta)c_F(\beta) + w_F(\beta), \;\; \beta = 1, \ldots, N \tag{3.6}$$

where $y_F(\beta)$, $c_F(\beta)$ and $w_F(\beta)$ are the received signals, the channel fading coefficients and the noise samples in the frequency domain, whose vector forms are given as $\mathbf{y}_F$, $\mathbf{c}_F$ and $\mathbf{w}_F$, respectively. The distributions of $c_F(\beta)$ and $w_F(\beta)$ are $\mathcal{CN}(0, 1)$ and $\mathcal{CN}(0, N_0)$, respectively, where N_0 is the noise variance in the frequency domain, which is equal to the noise variance in the time domain. The signal-to-noise ratio (SNR) is defined as $\rho = E_b/N_0$, where $E_b = (N + L)/m$ is the average transmitted energy per bit. For simplicity, the effect of CP on the spectral efficiency is ignored. Then, the spectral efficiency of the proposed scheme is obtained as

$$\eta = m/N \;\; \text{[bits/s/Hz]}. \tag{3.7}$$

Separate selection of MAPs and SAPs

Instead of joint selection, it is possible to determine MAPs and SAPs, separately. This scheme is called S-SuM-OFDM-IM. The only difference from SuM-OFDM-IM is the selection procedure of MAPs and SAPs. In this case, a total number of

$$p = \left\lfloor \log_2 \left(\binom{M}{2} \right) \right\rfloor + \left\lfloor \log_2 \left(\binom{n}{n/2} \right) \right\rfloor + \frac{n}{2} \log_2 Q, \tag{3.8}$$

bits are transmitted per subblock. As seen from Figure 3.2, the joint selection provides higher spectral efficiency than the separate one for varying Q values. However, in Section 3.3, we provide an interesting trade-off between error performance and spectral efficiency.

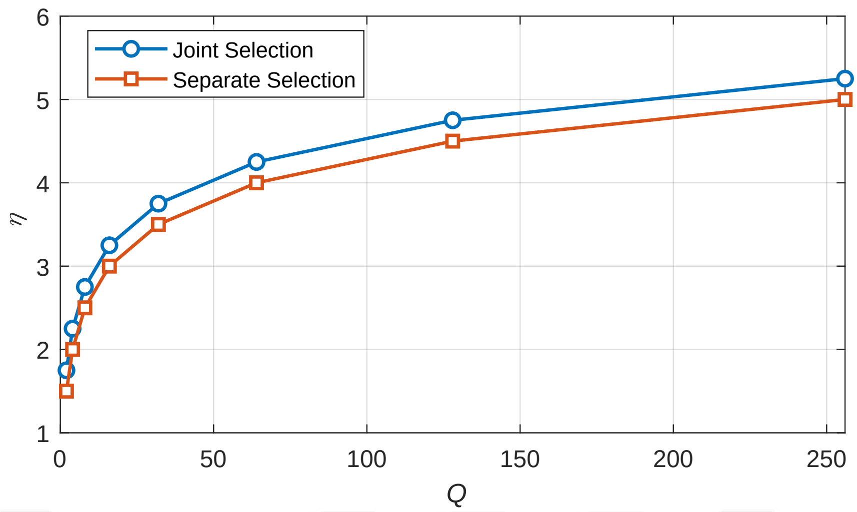

Figure 3.2: Spectral efficiency comparison of joint and separate selections of MAPs and SAPs for varying values of Q when $n = 4$ and $M = 4$.

3.1.2 Receiver

At the receiver side, after removing the CP, de-interleaving and performing FFT, ML detection can be considered to decode the αth subblock. The subblock set, which includes all possible subblock realizations, is defined as

$$\mathcal{S} = \{\mathbf{s}_1, \mathbf{s}_2, \ldots \mathbf{s}_{2^p}\}. \tag{3.9}$$

Then, ML detection rule for SuM-OFDM-IM is given as

$$\hat{\mathbf{s}} = \arg\min_{\mathbf{s}\in\mathcal{S}} \left\| \mathbf{y}_F^{(\alpha)} - \mathbf{c}_F^{(\alpha)} \odot \mathbf{s} \right\|^2, \tag{3.10}$$

where $\mathbf{y}_F^{(\alpha)}$ and $\mathbf{c}_F^{(\alpha)}$ and are the vectors of the received signals and the channel fading coefficients corresponding to αth subblock, respectively, and $\odot$ is the element-wise product.

The ML detection complexity per subblock is proportional to 2^p, therefore, it is not practical and efficient for large values of n, M and Q. Thus, a novel LLR-based reduced complexity ML detection algorithm is proposed for $n = 4$ and $n = 8$ as seen in Algorithm 1, which significantly reduces the detection complexity as discussed in Section 3.4. Since we perform repetition coding for data symbols, we present a modified LLR detector. This detector achieves the same performance as the ML detector since it searches for all possible MAP and SAP combinations.

The functions considered in Algorithm 1 are $\text{MAX}(a, b) = \max(a, b) + \ln(1 + e^{-|a-b|})$ and the combinatorial algorithm $\mathcal{I} = \text{combinatorics\_n2c}(c, d)$ that takes the integer c and the number of indices d as inputs and outputs the set of indices $\mathcal{I}$ [Basar et al., 2013a].

The major steps of Algorithm 1 are explained below:

1. The inputs of the algorithm are αth received subblock ($\mathbf{y}_F^{(\alpha)}$), the channel fading coefficients corresponding to αth subblock ($\mathbf{c}_F^{(\alpha)}$), noise power (N_0), the set of all modes ($\mathcal{M}$), the number of modes (M), modulation order (Q), the number of bits conveyed by IM (p_1) and the subblock size (n).

2. To determine the most likely MAP and SAP combination, LLR values are obtained between the lines (2-58). Specifically, between the lines (2-35), we provide a clever LLR calculation technique due to the unique symbol assignment strategy of our scheme. An iterative approach is applied between the lines (39-42) as in [Mao et al., 2017b].

3. By assigning $-\xi$, ($\xi >> 1$) to LLR values corresponding to illegal MAP and SAP combinations between the lines (59-65), we avoid them. Thus, these illegal values can not be selected.

4. Based on LLR values, MAP and SAP are jointly detected between the lines (66-69). For example, assuming $M = 4, n = 4$, we obtain

$$\mathbf{\Lambda} = \begin{bmatrix} \Lambda_{11} & \Lambda_{12} & \Lambda_{13} & \Lambda_{14} & \Lambda_{15} & \Lambda_{16} \\ \Lambda_{21} & \Lambda_{22} & \Lambda_{23} & \Lambda_{24} & \Lambda_{25} & \Lambda_{26} \\ \Lambda_{31} & \Lambda_{32} & \Lambda_{33} & \Lambda_{34} & \Lambda_{35} & \Lambda_{36} \\ \Lambda_{41} & \Lambda_{42} & \Lambda_{43} & \Lambda_{44} & \Lambda_{45} & \Lambda_{46} \\ \Lambda_{51} & \Lambda_{52} & \Lambda_{53} & \Lambda_{54} & \Lambda_{55} & \Lambda_{56} \\ \Lambda_{61} & \Lambda_{62} & -\xi & -\xi & -\xi & -\xi \end{bmatrix}, \tag{3.11}$$

where Λ_{ij} is the LLR value in ith row and jth column of the LLR matrix $\mathbf{\Lambda}$, which is formed between the lines (53-58). Columns and rows of $\mathbf{\Lambda}$ represents the possible MAPs and SAPs, respectively. As seen from (10), $\mathbf{\Lambda}$ includes LLR values for all possible MAP and SAP combinations; therefore, this detector provides the same error performance as the ML detector.

5. After detecting the active MAP and SAP, data symbols are decoded between the lines (70-80).

6. Finally, algorithm outputs the decoded data symbols ($\hat{\mathbf{x}}$) and decimal equivalent of IM bits ($\hat{d} = \hat{a}_1 + \binom{M}{2}\hat{a}_2$).

Remark (Generalization): To generalize the LLR-based detector for arbitrary n, only the following changes should be performed in Algorithm 1:

- The condition in line 17 is changed as $n \neq 4$ rather than $n = 8$.

- The lines between (70-80) are modified. For any values of n, a total of $n/2$ metric calculations are performed. If $\kappa \leq n/4$, the parameters $\hat{u}^{(2\kappa-1)}$, $\hat{u}^{(2\kappa)}$, and $\hat{v}^{(1)}$ are exploited to detect $\hat{x}_\kappa$, $\kappa = 1, \cdots, n/2$. If $\kappa > n/4$, the parameters $\hat{w}^{(2(\kappa-n/4)-1)}$, $\hat{w}^{(2(\kappa-n/4))}$, and $\hat{v}^{(2)}$ are exploited to detect $\hat{x}_\kappa$.

3.2 Mode Selection for SuM-OFDM-IM

In this section, we discuss our strategy for mode selection. According to [Wen et al., 2017], the optimal modes must maximize the minimum intra-mode distance (MIAD)

$$\begin{aligned}
&\epsilon_1 = \min_{\iota,\kappa \in \{1,\dots,2^p\}} \|\mathbf{S}_\iota - \mathbf{S}_\kappa\|_F^2, \\
&\text{s.t. } E\{\|\mathbf{S}\|_F^2\} = n \text{ and } \operatorname{rank}(\mathbf{S}_\iota - \mathbf{S}_\kappa) = 1,
\end{aligned} \tag{3.12}$$

where $\mathbf{S} = \operatorname{diag}(\mathbf{s})$, and the minimum inter-mode distance (MIRD)

$$\begin{aligned}
&\epsilon_2 = \min_{\iota,\kappa \in \{1,\dots,2^p\}} \|\mathbf{S}_\iota - \mathbf{S}_\kappa\|_F^2, \\
&\text{s.t. } E\{\|\mathbf{S}\|_F^2\} = n \text{ and } \operatorname{rank}(\mathbf{S}_\iota - \mathbf{S}_\kappa) = 2,
\end{aligned} \tag{3.13}$$

where $\mathbf{S}_\iota$ and $\mathbf{S}_\kappa$ are two different realizations of $\mathbf{S}$. For simplicity, we have removed superscript (α) in $\mathbf{S}^{(\alpha)}$, since all subblocks are identical. The modes can be created by partitioning PSK/QAM constellations as in [Wen et al., 2017] and it is proven

Algorithm 1 LLR-Based Reduced Complexity ML Detector ($n \in \{4, 8\}$)

Input: $\mathbf{y}_F^{(\alpha)}$, $\mathbf{c}_F^{(\alpha)}$, N_0, $\mathcal{M}$, M, Q, p_1, n

Output: $\hat{a_1}, \hat{a_2}, \hat{\mathbf{x}}$

$\mathbf{y} := \mathbf{y}_F^{(\alpha)}, \mathbf{c} := \mathbf{c}_F^{(\alpha)}$
for $i = 1$ **to** $\binom{n}{n/2}$ **do**
  $\mathcal{I}^{(i)}$:=combinatorics_n2c($i-1$,$n/2$)
  $j := 1$
  for $m = 1$ **to** M **do**
    for $h = 1$ **to** $n/4$ **do**
      for $q = 1$ **to** Q **do**
        for $z = 1$ **to** 2 **do**
          $\hat{\mathcal{I}} := \mathcal{I}^{(i,z+2(h-1))} + 1$
          $\delta_1^{(q,z+2(h-1))} := -|\mathbf{y}^{(\hat{\mathcal{I}})} - \mathbf{c}^{(\hat{\mathcal{I}})}\mathcal{M}^{(m,q)}|^2/N_0$
          $\delta_2^{(q,h)} := \delta_1^{(q,2h-1)} + \delta_1^{(q,2h)}$
        end for
      end for
    end for
    for $g_1 = 1$ **to** $n/4$ **do**
      for $g_2 = 1$ **to** g_1 **do**
        if $n = 8$ && $g_1 \neq g_2$ **then**
          for $q_1 = 1$ **to** Q **do**
            for $q_2 = 1$ **to** Q **do**
              $\gamma^{(j,i)} := \delta_2^{(q_1,g_1)} + \delta_2^{(q_2,g_2)}$
              $j := j + 1$
            end for
          end for
        else if $n = 4$ **then**
          for $q_1 = 1$ **to** Q **do**
            for $q_2 = 1$ **to** Q **do**
              $\gamma^{(j,i)} := \delta_2^{(q_1)} + \delta_2^{(q_2)}$
              $j := j + 1$
            end for
          end for
        end if
      end for
    end for
  end for
end for

for $i = 1$ **to** $\binom{n}{n/2}$ **do**
  $j := 1$
  for $m = 1$ **to** MQ^2 **with increments** Q^2 **do**
    $\Delta :=$MAX$(\gamma^{(m,i)}, \gamma^{(m+1,i)})$
    for $q = 2$ **to** $Q^2 - 1$ **do**
      $\Delta :=$MAX$(\Delta, \gamma^{(m+q,i)})$
    end for
    $\Gamma^{(j,i)} := \Delta$
    for $z = 1$ **to** $n/2$ **do**
      $\hat{\mathcal{I}} := \mathcal{I}^{(i,z)}$
      $\epsilon^{(z)} := -|\mathbf{y}^{(\hat{\mathcal{I}})}|^2/N_0$
    end for
    $\Gamma^{(j,i)} := \Gamma^{(j,i)} + \sum_{z=1}^{n/2} \epsilon^{(z)}$
    $j := j + 1$
  end for
end for
$\Gamma := \Gamma^{\mathrm{T}}$
for $v = 1$ **to** $\binom{M}{2}$ **do**
  $\tilde{\mathcal{I}} :=$combinatorics_n2c$(v-1, 2)$ +1
  for $r = 1$ **to** $\binom{n}{n/2}$ **do**
    $\mathbf{\Lambda}^{(r,v)} := \Gamma^{(r,\tilde{\mathcal{I}}^{(1)})} + \Gamma^{(\binom{n}{n/2}-r+1,\tilde{\mathcal{I}}^{(2)})}$
  end for
end for
for $a_1 = 0$ **to** $\binom{M}{2} - 1$ **do**
  for $a_2 = 0$ **to** $\binom{n}{n/2} - 1$ **do**
    if $(a_1 + \binom{M}{2}a_2 \geq 2^{p_1})$ **then**
      $\mathbf{\Lambda}^{(a_2+1,a_1+1)} := -\infty$
    end if
  end for
end for

$(\hat{a_2}, \hat{a_1}) = \arg\max_{a_1, a_2} \mathbf{\Lambda}^{(a_2, a_1)}$

$\hat{\mathbf{v}}$:=combinatorics_n2c($\hat{a_1} - 1$,2)+1

$\hat{\mathbf{u}}$:=combinatorics_n2c($\hat{a_2} - 1$,$n/2$)+1

$\hat{\mathbf{w}}$:=combinatorics_n2c($\binom{n}{n/2} - \hat{a_2} - 1$,$n/2$)+1

if $n = 8$ **then**

$\quad \hat{x}_1 := \arg\min_q \left\| [\mathbf{y}^{(\hat{\mathbf{u}}^{(1)})} \mathbf{y}^{(\hat{\mathbf{u}}^{(2)})}] - [\mathbf{c}^{(\hat{\mathbf{u}}^{(1)})} \mathbf{c}^{(\hat{\mathbf{u}}^{(2)})}] \mathcal{M}^{(\hat{\mathbf{v}}^{(1)}, q)} \right\|^2$

$\quad \hat{x}_2 := \arg\min_q \left\| [\mathbf{y}^{(\hat{\mathbf{u}}^{(3)})} \mathbf{y}^{(\hat{\mathbf{u}}^{(4)})}] - [\mathbf{c}^{(\hat{\mathbf{u}}^{(3)})} \mathbf{c}^{(\hat{\mathbf{u}}^{(4)})}] \mathcal{M}^{(\hat{\mathbf{v}}^{(1)}, q)} \right\|^2$

$\quad \hat{x}_3 := \arg\min_q \left\| [\mathbf{y}^{(\hat{\mathbf{w}}^{(1)})} \mathbf{y}^{(\hat{\mathbf{w}}^{(2)})}] - [\mathbf{c}^{(\hat{\mathbf{w}}^{(1)})} \mathbf{c}^{(\hat{\mathbf{w}}^{(2)})}] \mathcal{M}^{(\hat{\mathbf{v}}^{(2)}, q)} \right\|^2$

$\quad \hat{x}_4 := \arg\min_q \left\| [\mathbf{y}^{(\hat{\mathbf{w}}^{(3)})} \mathbf{y}^{(\hat{\mathbf{w}}^{(4)})}] - [\mathbf{c}^{(\hat{\mathbf{w}}^{(3)})} \mathbf{c}^{(\hat{\mathbf{w}}^{(4)})}] \mathcal{M}^{(\hat{\mathbf{v}}^{(2)}, q)} \right\|^2$

$\quad \hat{\mathbf{x}} = [\hat{x}_1 \ \hat{x}_2 \ \hat{x}_3 \ \hat{x}_4]$

else if $n = 4$ **then**

$\quad \hat{x}_1 := \arg\min_q \left\| [\mathbf{y}^{(\hat{\mathbf{u}}^{(1)})} \mathbf{y}^{(\hat{\mathbf{u}}^{(2)})}] - [\mathbf{c}^{(\hat{\mathbf{u}}^{(1)})} \mathbf{c}^{(\hat{\mathbf{u}}^{(2)})}] \mathcal{M}^{(\hat{\mathbf{v}}^{(1)}, q)} \right\|^2$

$\quad \hat{x}_2 := \arg\min_q \left\| [\mathbf{y}^{(\hat{\mathbf{w}}^{(1)})} \mathbf{y}^{(\hat{\mathbf{w}}^{(2)})}] - [\mathbf{c}^{(\hat{\mathbf{w}}^{(1)})} \mathbf{c}^{(\hat{\mathbf{w}}^{(2)})}] \mathcal{M}^{(\hat{\mathbf{v}}^{(2)}, q)} \right\|^2$

$\quad \hat{\mathbf{x}} = [\hat{x}_1 \ \hat{x}_2]$

end if

return $\hat{a_1}, \hat{a_2}, \hat{\mathbf{x}}$

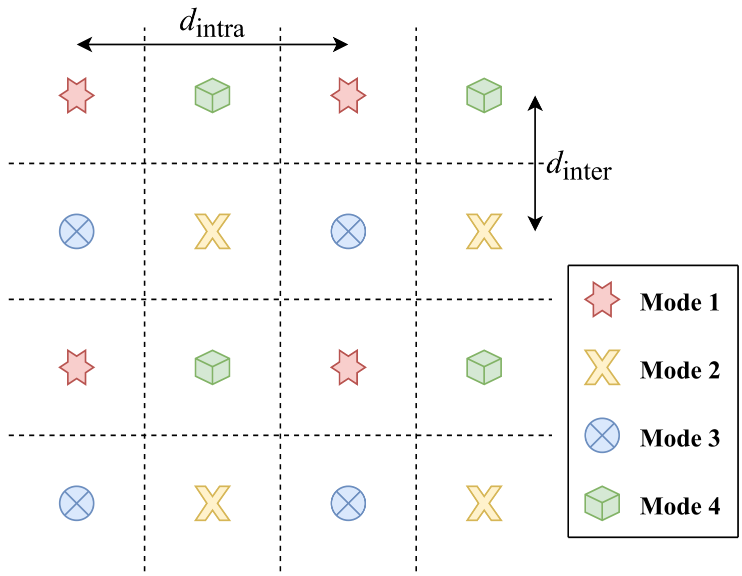

Figure 3.3: Partition of 16-QAM constellation for $M = 4$ and $Q = 4$.

that QAM constraint performs better than PSK constraint for $MQ > 4$. Therefore, we focus on only QAM constellation for our system model:

- QAM constraint to maximize MIRD:

$$d_{\text{inter}}(M,Q) = \begin{cases} 2\sqrt{\frac{6}{5QM-4}}, & \text{for rectangular } MQ\text{−QAM} \\ \sqrt{\frac{6}{QM-1}}, & \text{for square } MQ\text{−QAM} \end{cases} \tag{3.14}$$

- QAM constraint to maximize MIAD:

$$d_{\text{intra}}(M,Q) = \begin{cases} d_{\text{inter}}(M,Q)\frac{\sqrt{5M}}{2}, & \text{for rectangular } MQ\text{−QAM } (Q=2) \\ d_{\text{inter}}(M,Q)\sqrt{M}, & \text{otherwise} \end{cases} \tag{3.15}$$

- QAM constraint to maximize MIAD for $MQ >> 1$:

$$d_{\text{intra}}(M,Q) \approx d_{\text{intra}}(Q) = \begin{cases} 2\sqrt{\frac{6}{5Q}}, & \text{for rectangular } MQ\text{−QAM } (Q \neq 2) \\ \sqrt{\frac{6}{Q}}, & \text{otherwise} \end{cases} \tag{3.16}$$

with these constraints, modes can be obtained by partitioning QAM constellations for given parameters (M,Q). For example, for $M = 4, Q = 4$, the optimal modes for 16-QAM can be selected as in Figure 3.3, where $d_{\text{inter}} = 0.6325$ and $d_{\text{intra}} = 1.2649$ from (3.14) and (3.15), respectively.

3.3 Performance Analysis

In this section, we derive an upper bound on the BER of the SuM-OFDM-IM system employing ML detection. From (3.10), the conditional pairwise error probability (CPEP), which is defined as the probability of transmitting $\mathbf{S}$ and erroneously detecting $\hat{\mathbf{S}}$ conditioned on $\mathbf{c}_F$, is given as:

$$\Pr(\mathbf{S} \to \hat{\mathbf{S}}|\mathbf{c}_F) = \mathcal{Q}\left(\sqrt{\frac{\rho}{2}\left\|(\mathbf{S}-\hat{\mathbf{S}})\mathbf{c}_F\right\|^2}\right). \tag{3.17}$$

Then, by approximating $\mathcal{Q}(x) \approx \frac{e^{-x^2/2}}{12} + \frac{e^{-2x^2/3}}{4}$, the unconditioned PEP (UPEP) can be obtained as in [Basar et al., 2013a]:

$$\begin{aligned} \Pr\big(\mathbf{S} \to \hat{\mathbf{S}}\big) &= E_{\mathbf{c}_F}\{\Pr(\mathbf{S} \to \hat{\mathbf{S}}|\mathbf{c}_F)\} \\ &\approx \frac{1/12}{\det(\mathbf{I}_n + \rho_1\mathbf{A})} + \frac{1/4}{\det(\mathbf{I}_n + \rho_2\mathbf{A})}, \end{aligned} \tag{3.18}$$

where $\rho_1 = 1/(4N_0), \rho_2 = 1/(3N_0)$, and $\mathbf{A} = (\mathbf{S} - \hat{\mathbf{S}})^{\mathrm{H}}(\mathbf{S} - \hat{\mathbf{S}})$. Finally, according to the union bounding technique, the BER of SuM-OFDM-IM can be upper bounded by

$$P_e \leq \frac{1}{p2^p} \sum_{\mathbf{S}} \sum_{\hat{\mathbf{S}}} \Pr\big(\mathbf{S} \rightarrow \hat{\mathbf{S}}\big) e\big(\mathbf{S}, \hat{\mathbf{S}}\big), \tag{3.19}$$

where $\Pr(\mathbf{S} \rightarrow \hat{\mathbf{S}})$ is given by (3.18) and $e(\mathbf{S}, \hat{\mathbf{S}})$ represents the number of bit errors for the corresponding pairwise error event.

We have $\det(\mathbf{A}) = \prod_{\zeta=1}^{r} \lambda_\zeta(\mathbf{A})$ where $\lambda_\zeta(\mathbf{A})$ is the ζth eigenvalue of $\mathbf{A}$ and $r = \mathrm{rank}(\mathbf{A})$ determines the diversity order of the system, since P_e decays with r. At high SNR values, by ignoring $\mathbf{I}_n$ terms in (3.18), (3.19) can be simplified as follows:

$$P_e \leq \frac{\rho_1^{-r} + 3\rho_2^{-r}}{12p2^p} \sum_{\mathbf{S}} \sum_{\hat{\mathbf{S}}} \Big(\prod_{\zeta=1}^{r} \lambda_\zeta(\mathbf{A})\Big)^{-1} e\big(\mathbf{S}, \hat{\mathbf{S}}\big). \tag{3.20}$$

We investigate two cases: (i) erroneous detection of index bits and (ii) erroneous detection of a single or multiple data symbols while the index bits are decoded correctly. For case (i), due to our novel MAP and SAP selection strategy, we always obtain $r \geq 2$. For example, from Table 3.1, assume that $\mathbf{v} = [1, 2]$ is selected and $\hat{\mathbf{v}} = [1, 3]$ is decoded erroneously, which is the worst case error event due to overlapping index values of $\mathbf{v}$ and $\hat{\mathbf{v}}$. Even in this error event, r is obtained as 2 as in plain OFDM-IM systems [Basar et al., 2013a]. If $\mathbf{v}$ and $\hat{\mathbf{v}}$ have non-overlapping indices, r might be even equal to 3 or 4. To explain case (ii), we illustrate the following example. Assume that $n = 4$, $M = 4$, $Q = 4$ and $\mathbf{S} = \mathrm{diag}([\chi_{11}\chi_{11}\chi_{31}\chi_{31}])$, which is obtained as in (3.3), is transmitted and $\hat{\mathbf{S}} = \mathrm{diag}([\chi_{11}\ \chi_{11}\ \chi_{32}\ \chi_{32}])$ is erroneously detected, i.e, MAP and SAP are detected correctly; however, the second symbol is decoded erroneously ($\chi_{31} \rightarrow \chi_{32}$). Then, we obtain:

$$\mathbf{A} = \begin{bmatrix} 0 & 0 & 0 & 0 \\ 0 & 0 & 0 & 0 \\ 0 & 0 & 1.6 & 0 \\ 0 & 0 & 0 & 1.6 \end{bmatrix}, \tag{3.21}$$

where $r = \mathrm{rank}(\mathbf{A}) = 2$. As seen from this example, due to clever symbol assignment strategy of our scheme, even the erroneous detection of a single data symbol ensures

Table 3.2: Percentage of Error Events

(M, Q)	$r = 2$	$r = 3$	$r = 4$
$(4, 4)$	4.79%	15.07%	80.14%
$(8, 2)$	5.10%	14.95%	79.95%
$(4, 16)$	1.14%	4.02%	94.84%
$(16, 4)$	1.27%	3.92%	94.81%

a diversity order of 2. It can be easily shown that for all error events of this type, we again obtain at least $r = 2$.

To provide further insights on the performance of SuM-OFDM-IM, we obtain the percentage of error events with $r = 2, 3$ and 4 in Table 3.2 for varying (M, Q) by considering all possible error events for $n = 4$. It should be noted that the percentage of error events has a remarkable affect on the overall error performance of a system from (3.19). As it can be deduced from Table 3.2, since $r = 4$ is obtained much more frequently than other possible rank values, our proposed system is capable of providing a superior error performance. It can be seen from Table 3.2 that as the overall constellation size (MQ) increases, the percentage of $r = 4$ increases due to the increase in the number of data symbols. Because, when MAP and SAP are detected correctly and two data symbols are decoded erroneously, we obtain $r = 4$. Finally, in light of the above discussion, we obtain

$$\min_{\mathbf{s}, \hat{\mathbf{s}}} \operatorname{rank}(\mathbf{A}) = 2, \tag{3.22}$$

which proves that our system provides a diversity order of 2.

3.4 Simulation Results

In this section, Monte Carlo simulations are performed to compare the error performance of SuM-OFDM-IM with reference schemes. All simulations have been performed under frequency-selective Rayleigh fading channels and perfect channel estimation is assumed at the receiver side. OFDM parameters are adjusted to $N = 128$, $v = 10$ and $L = 16$ for all simulations. We define "OFDM-IM(n, k) and CI-OFDM-IM(n, k)" as k out of n subcarriers being active in a subblock, "DM-OFDM(n, k)" as

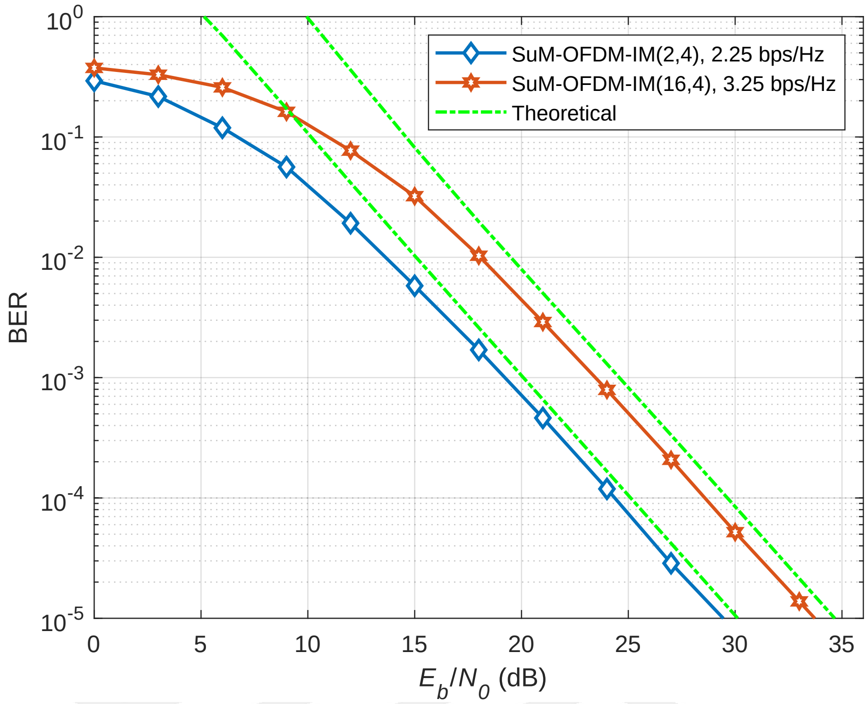

Figure 3.4: Theoretical BER upper bound of SuM-OFDM-IM with simulation results.

k subcarriers out of n exploiting the primary M-ary PSK/QAM constellation, "MM-OFDM-IM(Q, M), SuM-OFDM-IM(Q, M), and S-SuM-OFDM-IM(Q, M)" with M modes, each including Q symbols.

As shown in Figure 3.4, the theoretical BER curve obtained by (3.19) is an accurate upper bound for simulation results of SuM-OFDM-IM for varying parameters (Q, M). Since (3.18) is an approximation, as spectral efficiency increases, the number of terms in (3.19) also increases; therefore, the gap between simulation and theoretical curves does not diminish.

It is observed from Figure 3.5 that SuM-OFDM-IM and S-SuM-OFDM-IM have superior BER performances over reference systems for approximately the same spectral efficiency. As seen from Figure 3.5, SuM-OFDM-IM and S-SuM-OFDM-IM outperform classical OFDM, OFDM-IM, DM-OFDM and MM-OFDM-IM. Additionally, at a BER value of 10^{-5}, SuM-OFDM-IM provides almost 10 dB gain over MM-OFDM-IM although providing a 12.5% higher spectral efficiency. It is also shown that LLR-based reduced ML detector provides the same error performance

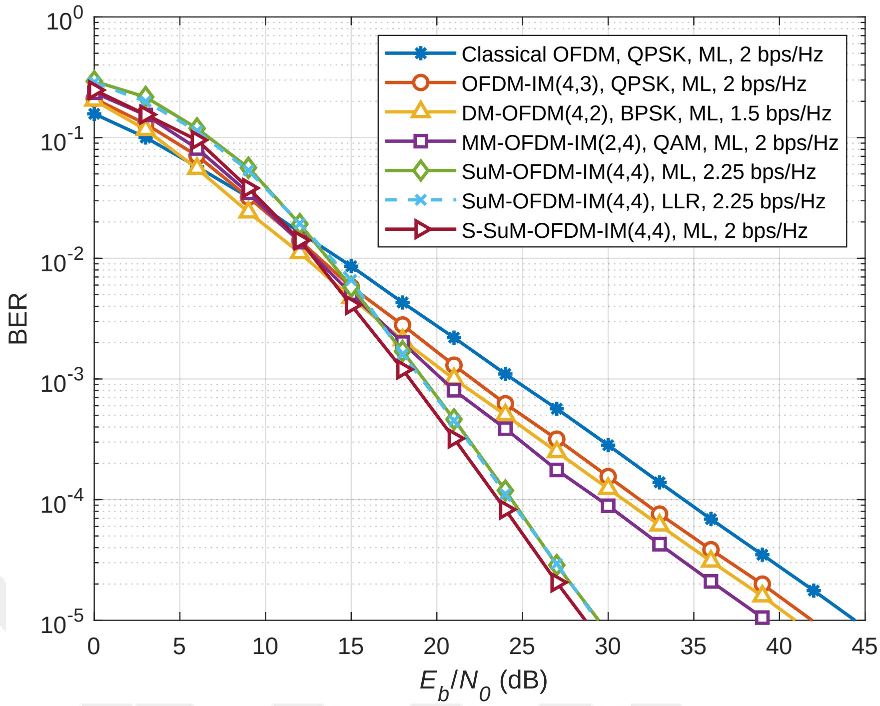

Figure 3.5: Error performance comparison of SuM-OFDM-IM and S-SuM-OFDM-IM with reference systems.

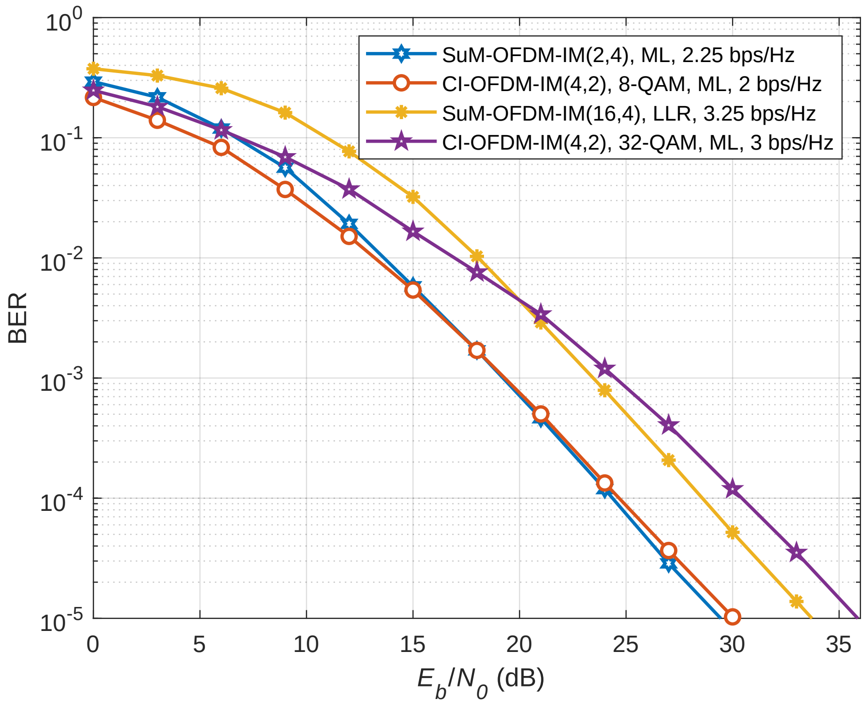

Figure 3.6: Error performance comparison of SuM-OFDM-IM with CI-OFDM-IM.

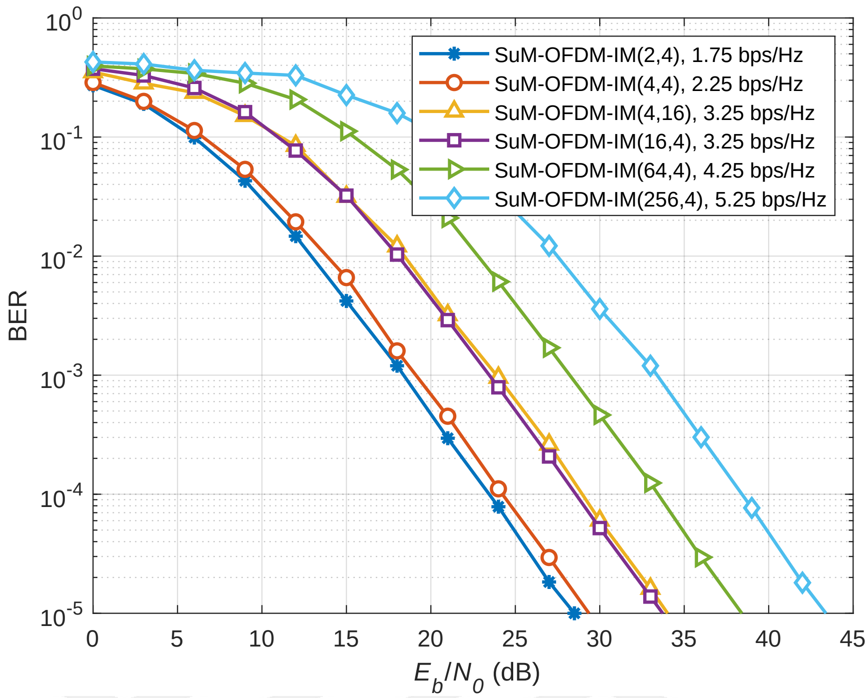

Figure 3.7: Error performance of SuM-OFDM-IM for different spectral efficiencies with LLR detector for $n = 4$.

as that of the ML detector. Although SuM-OFDM-IM performs only slightly worse in terms of error performance than S-SuM-OFDM-IM, its spectral efficiency is 12.5% higher.

In Figure 3.6, SuM-OFDM-IM is compared with CI-OFDM-IM, which also provides a second order diversity gain. First, we consider 2 and 2.25 bps/Hz for CI-OFDM-IM and SuM-OFDM-IM, respectively. SuM-OFDM-IM provides a marginal gain at a BER value of 10^{-5} than CI-OFDM-IM despite a 12.5% improvement in terms of spectal efficiency. Moreover, we consider 3 and 3.25 bps/Hz for CI-OFDM-IM and SuM-OFDM-IM, respectively. SuM-OFDM-IM is able to provide a noticeable gain at a BER value of 10^{-5} than CI-OFDM-IM despite yielding a 8.33% higher spectral efficiency. It can be clearly concluded that the performance difference between SuM-OFDM-IM and CI-OFDM-IM increases with spectral efficiency.

In Figure 3.7, the error performance of SuM-OFDM-IM with varying (Q, M) parameters is given for different spectral efficiency values and $n = 4$. LLR-based reduced complexity ML detector is employed in all cases. As seen from Figure 3.7,

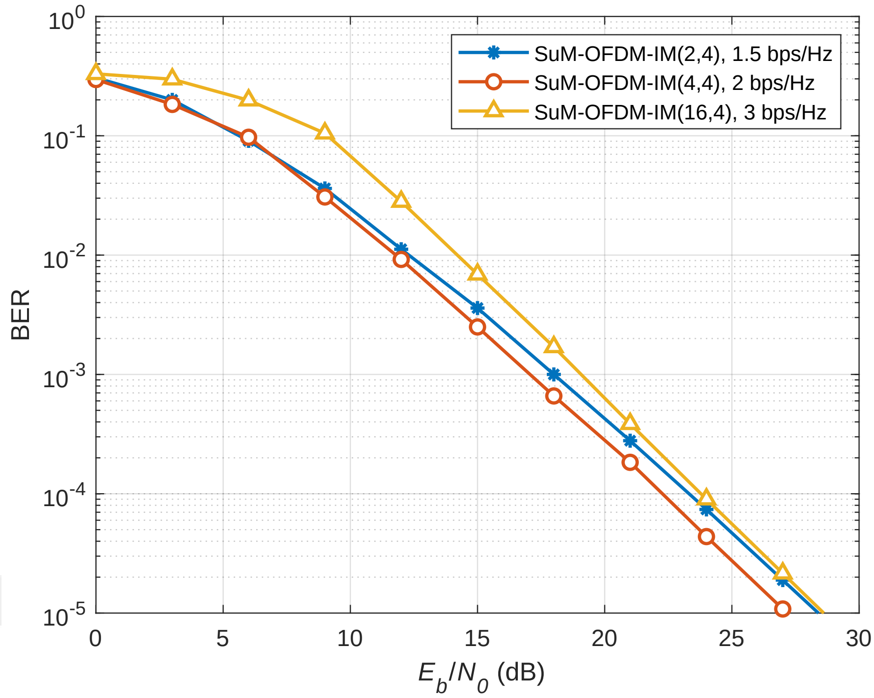

Figure 3.8: Error performance of SuM-OFDM-IM for different spectral efficiencies with LLR detector for $n = 8$.

the slopes of the curves are equal and the error performance degrades with increasing spectral efficiency.

Error performance of SuM-OFDM-IM for varying parameters (Q, M) is shown in Figure 3.8 where $n = 8$. We observe that the error performance is inversely proportional to the size of the constellation. As Q increases, the percentage of higher rank values increases and it can be seen from Figure 3.8 that at a BER value of 10^{-5}, the performances of schemes with 2 bps/Hz and 3 bps/Hz are close to each other. By comparing Figures 3.7 and 3.8 to investigate the effect of n on the BER performance, it can readily be deduced that the system with $n = 8$ and 3 bps/Hz outperforms the system with $n = 4$ and 3.25 bps/Hz. This is because r may even be equal to 8 when $n = 8$, resulting in an improvement in error performance; nevertheless, the complexity increases proportional to n as seen in Table 3.3. Additionally, it is more challenging to reach a higher spectral efficiency for $n = 8$ compared to $n = 4$ by (3.8). Therefore, we introduce interesting trade-offs among spectral efficiency, decoding complexity and error performance.

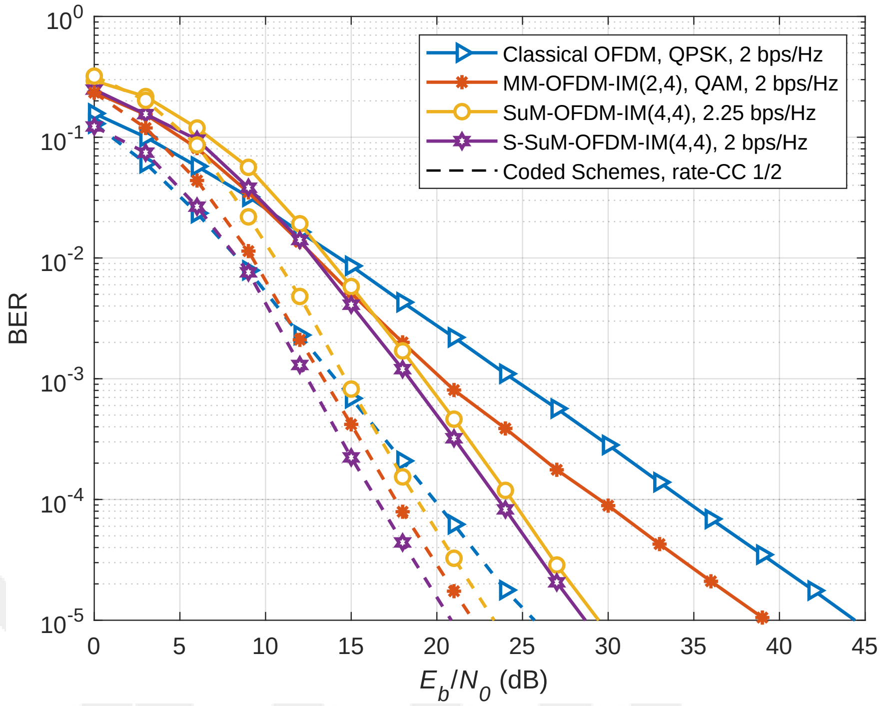

Figure 3.9: Uncoded/Coded performance of OFDM, MM-OFDM-IM, SuM-OFDM-IM, and S-SuM-OFDM-IM.

In Figure 3.9, the error performance curves of uncoded and coded OFDM, MM-OFDM-IM, SuM-OFDM-IM, and S-SuM-OFDM-IM are given. For all coded schemes, the rate-1/2 convolutional code (CC) with octal generator sequence of [1, 3] and a bit-interleaver are employed. As seen from Figure 3.9, SuM-OFDM-IM and S-SuM-OFDM-IM outperform OFDM at a BER value of 10^{-5} also with channel coding. Moreover, it is observed that the difference between coded SuM-OFDM-IM and coded OFDM increases for higher SNR values due to different slopes of their curves. While the advantage of SuM-OFDM-IM is not significant compared to MM-OFDM-IM for this specific case, SuM-OFDM-IM can also be a candidate for potential future uncoded applications due to its diversity gain. However, in the presence of coding, S-SuM-OFDM-IM outperforms MM-OFDM-IM. Therefore, we present an interesting trade-off between error performance and spectral efficiency for SuM-OFDM-IM and S-SuM-OFDM-IM.

Table 3.3: Decoding Complexity Comparison

System	**Detector**	**Complexity Order**
OFDM	ML	$\mathcal{O}(Q)$
OFDM-IM [Basar et al., 2013a]	Red. Comp. ML	$\mathcal{O}(Q)$
DM-OFDM [Mao et al., 2017b]	Suboptimal	$\mathcal{O}(Q_A + Q_B)$
MM-OFDM-IM [Wen et al., 2017]	Suboptimal	$\mathcal{O}(\frac{Qn}{2} + \frac{Q}{2})$
CI-OFDM-IM [Basar, 2015]	Red. Comp. ML	$\mathcal{O}(Q^2)$
SuM-OFDM-IM	Red. Comp. ML	$\mathcal{O}(\binom{n}{n/2}\frac{QM}{2})$
S-SuM-OFDM-IM	Red. Comp. ML	$\mathcal{O}(\binom{n}{n/2}\frac{QM}{2})$

3.4.1 Complexity Analysis

In this subsection, we analyze the decoding complexity order of SuM-OFDM-IM and make comparisons with the reference systems. A comparison for complexity per subcarrier in terms of complex multiplications (CMs), is given in Table 3.3, where Q_A and Q_B stand for the primary and secondary constellations for DM-OFDM, respectively, and k is the number of active subcarriers in a CI-OFDM-IM subblock. Due to space limitation, we do not give the design of LLR-based reduced complexity ML detection for S-SuM-OFDM-IM, however, it can be designed as in Algorithm 1 in a similar manner. In this case, the complexity order of SuM-OFDM-IM and S-SuM-OFDM-IM would be equivalent as seen in Table 3.3.

To further elaborate on the complexity order of the proposed system and reference systems, we give a numerical example in Table 3.4. For a fair comparison, the parameters in Figures 3.6 and 3.5 are considered for CI-OFDM-IM with 2 bps/Hz and other systems, respectively. As seen from Table 3.4, we provide an interesting trade-off among complexity and error performance. With these specific parameters, although SuM-OFDM-IM is the second most complex system, it provides a superior error performance as seen in Figures 3.5 and 3.6. It should also be noted that the LLR-based reduced complexity ML detector dramatically reduces the complexity

Table 3.4: A Numerical Example For Complexity Comparison

System	Detector	CMs per subcarrier
OFDM	ML	4
OFDM-IM	Red. Comp. ML	4
DM-OFDM	Suboptimal	4
MM-OFDM-IM	Suboptimal	5
CI-OFDM-IM	Red. Comp. ML	64
SuM-OFDM-IM	Red. Comp. ML	48
SuM-OFDM-IM	ML	128

Figure 3.10: Experimental testbed at CoreLab [CoreLab, 2020] with USRP modules.

of SuM-OFDM-IM when compared to the ML detector. Moreover, the LLR-based and low-complexity ML detector is not significantly complex for varying n, Q and M values. For example, for a spectral efficiency of 1.75 bps/Hz, only 24 CMs per subcarrier are required. Hence, SuM-OFDM-IM is applicable in practice with the proposed low-complexity detector.

3.5 Experimental Results

In this section, we evaluate the performance of SuM-OFDM-IM in a practical setup and give the models of the transmitter and receiver testbeds. As seen from Figure 3.10, two USRP 2943 modules are used for transmitter and receiver nodes and an OctoClock CDA-2990 that generates 10 MHz clock signal for synchronization. For programming, virtual instrument (VI) components of LabVIEW are utilized.

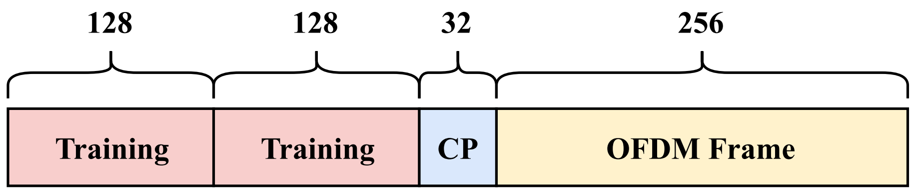

Figure 3.11: Overall symbol structure.

Table 3.5: Experimental Parameters

Carrier Frequency	2.45 GHz
I/Q data rate	5×10^5 samples/sec
Sampling rate (f_s)	6.25×10^5 samples/sec
Number of data subcarriers	125
Number of pilot tones	25
Zero padding/FFT size (N)	106/256
CP size (L)	32
Distance between terminals	225 cm

3.5.1 Transmitter Details

Channel Estimation

Comb-type channel estimation method with one dimensional linear interpolation is employed to estimate the channel as in [Gokceli et al., 2017]. A certain number of subcarriers are assigned as pilot tones. In this experiment, we consider the ratio of data to pilot subcarriers as 4, i.e, for 4 data subcarriers, one pilot tone is employed.

Symbol Structure

Overall symbol structure is shown in Figure 3.11. We insert two identical training sequences with 128 samples for both TO and CFO estimation at the beginning of the symbol. In the OFDM frame, the initial 53, the center and the final 52 subcarriers are set to 0. A total 150 subcarriers are assigned to data and pilot tones. Since the ratio of data subcarriers to pilot tones is 4, we have a total number of 125 data and

25 pilot subcarriers. After the IFFT operation, a CP with 32 samples is inserted in the time domain. Experiment parameters are summarized in Table 3.5. The bandwidth, subcarrier spacing and symbol duration are 500 kHz, 3.333 kHz and 0.3 ms, respectively.

3.5.2 Receiver Details

In the presence of CFO (ε) and TO (γ), the received baseband signal in time domain can be given as:

$$y_T(\tau) = \frac{1}{N}\sum_{\beta=0}^{N-1} s_F(\beta)c_F(\beta)e^{j2\pi(\beta+\varepsilon)(\tau+\gamma)/N} + w_T(\tau), \tag{3.23}$$

where $w_T(\tau)$, $\tau = 1, 2, \cdots, N$ represent the noise samples in the time domain, whose vector form is given as $\mathbf{w}_T = \text{IFFT}\{\mathbf{w}_F\}$.

CFO and TO Estimation

After receiving signals, by using consecutive and identical training sequences, timing offset (TO) and carrier frequency offset (CFO) are estimated in time and frequency domain, respectively. By using sliding windows, which have the same lengths as the training sequence, the similarity between two blocks is obtained by autocorrelation [Cho et al., 2010]. Hence, TO can be ML estimated as:

$$\hat{\gamma} = \arg\max_{\gamma}\left\{\frac{\left|\sum_{i=\gamma}^{N/2-1+\gamma} y_T(\tau+i)y_T^*(\tau+N/2+i)\right|^2}{\left|\sum_{i=\gamma}^{N/2-1+\gamma} y_T(\tau+N/2+i)\right|^2}\right\}. \tag{3.24}$$

After obtaining the start of the frame (TO), by taking FFT of training sequences, CFO is estimated in the frequency domain with the technique proposed by Moose [Moose, 1994] as follows:

$$\hat{\varepsilon} = \frac{1}{2\pi}\tan^{-1}\left\{\frac{\sum_{\beta=0}^{N-1}\Im\{T_1^*(\beta)T_2(\beta)\}}{\sum_{\beta=0}^{N-1}\Re\{T_1^*(\beta)T_2(\beta)\}}\right\}, \tag{3.25}$$

where $T_l, l = 1, 2$ is the lth received training sequence in the frequency domain. Finally, the CP is removed and the CFO is compensated.

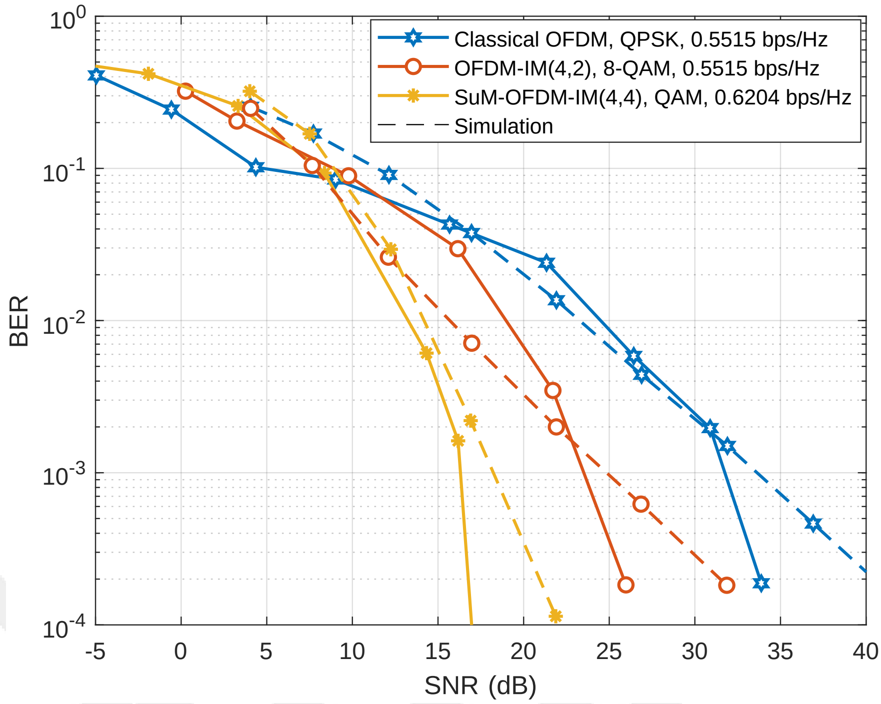

Figure 3.12: Error performance of OFDM, OFDM-IM and SuM-OFDM-IM under a practical setup and with computer simulation.

Channel Estimation

After performing FFT, data and pilot tones are separated. By employing pilot tones, channel coefficients are estimated with one-dimensional linear interpolation as in [Gokceli et al., 2017]. Finally, the estimated channel coefficients are fed into the detector.

SNR Estimation

For SNR estimation, the method proposed in [Arslan and Reddy, 2003] is considered. The estimated SNR values for all target systems can be given as

$$\mathrm{SNR} = \frac{\sum_{\beta=1}^{N} |y_F(\beta)|^2}{\sum_{\beta=1}^{N} |y_F(\beta) - s_F(\beta)h_F(\beta)|^2}. \tag{3.26}$$

3.5.3 Error Performance

In this subsection, the error performance of SuM-OFDM-IM is compared with OFDM and OFDM-IM under a practical setup. ML detector is employed for all schemes. A three-tap Rician channel with uniform power delay profile and K-factor of 10 dB is considered to compare simulation results with experimental results similar to [Gokceli et al., 2017]. As seen from Figure 3.12, SuM-OFDM-IM outperforms OFDM and OFDM-IM in terms of error performance even though providing a 12.5% higher spectral efficiency. These experimental results are also consistent with the simulation results.

Chapter 4

OFDM WITH POWER DISTRIBUTION INDEX MODULATION

In this chapter, the system models, performance analyses, and simulation results of OFDM-PIM and OFDM-I/Q-PIM schemes are given.

4.1 System model of OFDM-PIM

The transmitter structure of OFDM-PIM is given in Figure 4.1. A total number of m bits are conveyed with the transmission of each OFDM block. These bits are split into G groups. Each group contains $p = m/G = p_1 + p_2$ bits and these bits form a subblock with length $n = N/G$, where N is the size of the FFT. For the creation of gth subblock $\mathbf{s}_g$, firstly, $p_1 = \frac{n}{2}\log_2(M)$ bits determine the data symbols $\mathbf{x}_g = [x_g(1), x_g(2), \cdots, x_g(n/2)], g = 1, \cdots, G$ from the M-ary signal constellation. The average power of the signal constellation is normalized to unity. Two power levels are defined, high (P_1) and low (P_2), where $P_1 > P_2$ and $P_1 + P_2 = 2$ under normalized subcarrier powers. The selection strategy of P_1 and P_2 is given in the following section. Secondly, $p_2 = \lfloor \log_2 \binom{n}{n/2} \rfloor$ bits determine the indices of high power subcarriers $\mathbf{i}_g = [i_g(1), i_g(2), \cdots, i_g(n/2)]$ using combinatorial method as in [Basar et al., 2013a]. The remaining subcarrier indices are assigned a low power and are represented as $\mathbf{k}_g = [k_g(1), k_g(2), \cdots, k_g(n/2)]$. Then, the data symbols vector $\mathbf{x}_g$ is multiplied with $\sqrt{P_1}$ and $\sqrt{P_2}$ and the new data symbols vectors $\bar{\mathbf{x}}_g = \sqrt{P_1}[x_g(1), x_g(2), \cdots, x_g(n/2)]$ and $\tilde{\mathbf{x}}_g = \sqrt{P_2}[x_g(1), x_g(2), \cdots, x_g(n/2)]$ are obtained. The entries of $\bar{\mathbf{x}}_g$ and $\tilde{\mathbf{x}}_g$ are placed into the subblock with the entries of $\mathbf{i}_g$ and $\mathbf{k}_g$, respectively. Consequently, a total number of

$$p = p_1 + p_2 = \frac{n}{2}\log_2(M) + \lfloor \log_2 \binom{n}{n/2} \rfloor, \tag{4.1}$$

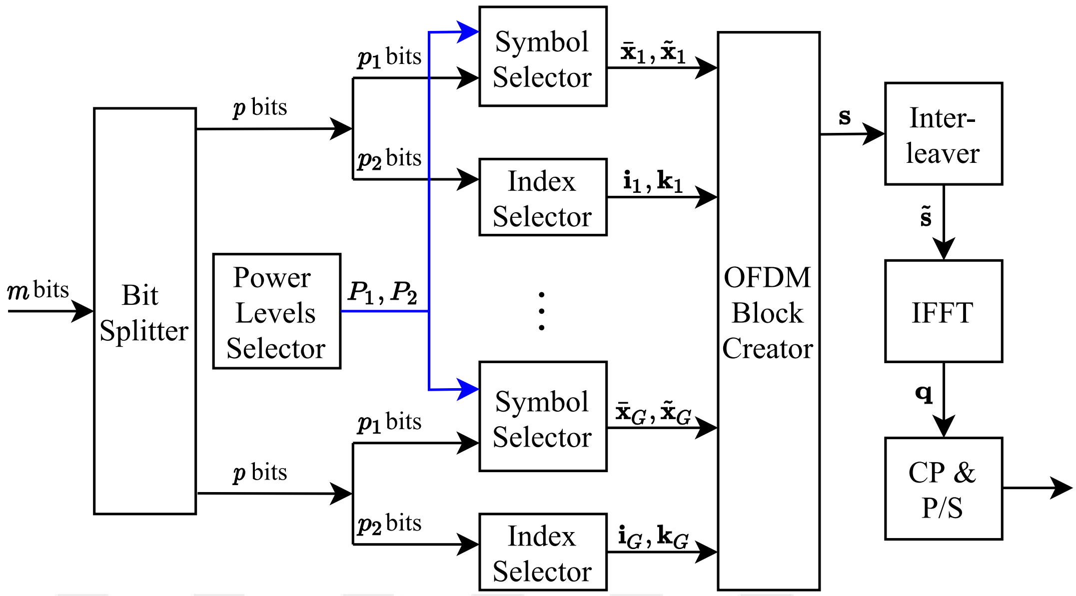

Figure 4.1: Transmitter structure of OFDM-PIM.

bits are transmitted per subblock. For convenience, we provide an example for the creation of $\mathbf{s}_g$.

Example: Assume that $n = 4$, $M = 4$ with Gray mapping and we transmit the bit sequence of $\{10|00|01\}$. The first $p_1 = 2\log_2(4) = 4$ bits $\{10|00\}$ determine the data symbols as $\mathbf{x}_g = [-1, j]$. Later, the power allocated data vectors are obtained as $\bar{\mathbf{x}}_g = [-\sqrt{P_1}, \sqrt{P_1}j]$ and $\tilde{\mathbf{x}}_g = [-\sqrt{P_2}, \sqrt{P_2}j]$. Then, $p_2 = \lfloor \log_2 \binom{4}{2} \rfloor = 2$ bits $\{01\}$ determine the indices of high power subcarriers as $\mathbf{i}_g = [1, 3]$ and the remaining ones are the indices of low power subcarriers $\mathbf{k}_g = [2, 4]$. Finally, $\mathbf{s}_g$ can be given as:

$$\mathbf{s}_g = [-\sqrt{P_1} \;\; -\sqrt{P_2} \;\; \sqrt{P_1}j \;\; \sqrt{P_2}j]^{\mathrm{T}}, \tag{4.2}$$

The power distribution for the example subblock given in (2) is shown in Figure 4.2.

By applying the same procedures for all subblocks, the main OFDM block $\mathbf{s} = [\mathbf{s}_1^{\mathrm{T}} \mathbf{s}_2^{\mathrm{T}} \cdots \mathbf{s}_G^{\mathrm{T}}]^{\mathrm{T}}$ is created. A block-type interleaver is performed as in [Basar et al., 2013a] and the interleaved OFDM block $\tilde{\mathbf{s}}$ is obtained. IFFT is applied to $\tilde{\mathbf{s}}$ and time-domain OFDM block $\mathbf{q}$ is obtained. Then, a CP of length C is added, parallel-to-serial and digital-to-analog conversions are performed. The resulting signal is transmitted through a T-tap frequency selective Rayleigh fading channel whose elements follow $\mathcal{CN}(0, \frac{1}{T})$ distribution. During the transmission of an OFDM block,

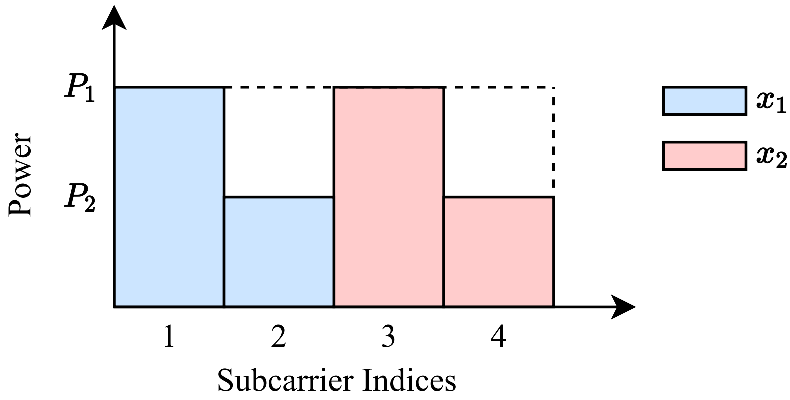

Figure 4.2: Power distribution for the example subblock given in (4.2).

we assume that channel remains constant $C > T$. At the receiver, FFT operation is applied. Finally, in the frequency domain, the equivalent input-output relationship can be given as:

$$\tilde{\mathbf{y}} = \tilde{\mathbf{H}}\tilde{\mathbf{s}} + \mathbf{n}, \tag{4.3}$$

where $\tilde{\mathbf{y}}$, $\tilde{\mathbf{H}} = \text{diag}(\tilde{\mathbf{h}})$, and $\mathbf{n}$ are the received signal vector, the channel matrix, and the noise vector in the frequency domain, respectively, where diag$(\cdot)$ is diagonalization operation. The distributions of the elements of $\mathbf{h}$ and $\mathbf{n}$ are $\mathcal{CN}(0, 1)$ and $\mathcal{CN}(0, N_0)$, respectively, where N_0 is the noise variance. The SNR is defined as $\lambda = E_b/N_0$ where, $E_b = (N + C)/m$ is the average transmitted energy per bit. A block-type deinterleaver is applied to $\tilde{\mathbf{y}}$ and $\tilde{\mathbf{h}}$. We obtain the deinterleaved received signal vector $\mathbf{y}$ and channel vector $\mathbf{h}$.

At the receiver, after removing CP and deinterleaving, received signal and channel vectors are split into G groups and represented as $\mathbf{y} = [\mathbf{y}_1^{\mathrm{T}}\mathbf{y}_2^{\mathrm{T}} \cdots \mathbf{y}_G^{\mathrm{T}}]^{\mathrm{T}}$ and $\mathbf{h} = [\mathbf{h}_1^{\mathrm{T}}\mathbf{h}_2^{\mathrm{T}} \cdots \mathbf{h}_G^{\mathrm{T}}]^{\mathrm{T}}$, respectively. Subblock wise ML detector is exploited to decode the gth subblock with the set $\mathcal{Z} \in \{\mathbf{z}_1, \mathbf{z}_2, \cdots, \mathbf{z}_{2^p}\}$ that includes all possible subblock realizations:

$$\hat{\mathbf{s}}_g = \arg\min_{\mathbf{z}\in\mathcal{Z}} \|\mathbf{y}_g - \mathbf{H}_g\mathbf{z}\|^2, \tag{4.4}$$

where $\mathbf{H}_g = \text{diag}(\mathbf{h}_g) \in \mathbb{C}^{n\times n}$. The complexity order of the ML detection can be given as $\mathcal{O}(2^p)$.

4.2 Extension To IQ

In order to double the number of bits transmitted by IM, we propose OFDM-I/Q-PIM which applies PIM for both in-phase and quadrature components of the data symbols, separately. After determining data symbols $\bar{\mathbf{x}}_g, \tilde{\mathbf{x}}_g$ as in OFDM-PIM, $\tilde{p}_2 = 2\lfloor \log_2 \binom{n}{n/2} \rfloor$ number of bits determine the subcarrier indices as $\mathbf{i}_g^{\mathcal{I}} = [i_g^{\mathcal{I}}(1), i_g^{\mathcal{I}}(2), \cdots, i_g^{\mathcal{I}}(n/2)]$ and $\mathbf{i}_g^{\mathcal{Q}} = [i_g^{\mathcal{Q}}(1), i_g^{\mathcal{Q}}(2), \cdots, i_g^{\mathcal{Q}}(n/2)]$ for in-phase and quadrature parts of these symbols, respectively. The remaining subcarrier indices are represented as $\mathbf{k}_g^{\mathcal{I}} = [k_g^{\mathcal{I}}(1), k_g^{\mathcal{I}}(2), \cdots, k_g^{\mathcal{I}}(n/2)]$ and $\mathbf{k}_g^{\mathcal{Q}} = [k_g^{\mathcal{Q}}(1), k_g^{\mathcal{Q}}(2), \cdots, k_g^{\mathcal{Q}}(n/2)]$. Then, the entries of $\Re\{\bar{\mathbf{x}}_g\}$ and $\Re\{\tilde{\mathbf{x}}_g\}$ are placed into the subblock with the entries of $\mathbf{i}_g^{\mathcal{I}}$ and $\mathbf{k}_g^{\mathcal{I}}$, respectively, and the entries of $\Im\{\bar{\mathbf{x}}_g\}$ and $\Im\{\tilde{\mathbf{x}}_g\}$ are placed into the subblock with the entries of $\mathbf{i}_g^{\mathcal{Q}}$ and $\mathbf{k}_g^{\mathcal{Q}}$, respectively. Consequently, a total number of

$$\tilde{p} = p_1 + \tilde{p}_2 = \frac{n}{2}\log_2(M) + 2\lfloor \log_2 \binom{n}{n/2} \rfloor, \tag{4.5}$$

bits are transmitted per subblock. At the receiver, ML detection in (4.4) is exploited to detect symbols and indices.

For simplicity, we ignore the effect of CP on spectral efficiency. Then, the spectral efficiencies of OFDM-PIM and OFDM-I/Q-PIM are obtained as $\eta = pG/N$ and $\eta = \tilde{p}G/N$, respectively.

4.3 Performance Analyses

Since error performance is identical for all subblocks, the PEP events of a single subblock are investigated. Assume that $\mathbf{Z} = \mathrm{diag}(\mathbf{z})$ is transmitted and $\hat{\mathbf{Z}} = \mathrm{diag}(\hat{\mathbf{z}})$ is erroneously detected. Note that from (4.3), CPEP is given as:

$$\mathrm{P}(\mathbf{Z} \to \hat{\mathbf{Z}} | \mathbf{h}_g) = Q\left(\sqrt{\frac{\Delta}{2N_0}}\right), \tag{4.6}$$

where $\Delta = ||(\mathbf{Z} - \hat{\mathbf{Z}})\mathbf{h}_g||_F^2 = \mathbf{h}_g^{\mathrm{H}}\mathbf{A}\mathbf{h}_g$ and $\mathbf{A} = (\mathbf{Z} - \hat{\mathbf{Z}})^{\mathrm{H}}(\mathbf{Z} - \hat{\mathbf{Z}})$. By employing the approximation $Q(x) \approx \frac{1}{12}e^{-x^2/2} + \frac{1}{4}e^{-2x^2/3}$, the UPEP of the OFDM-PIM scheme

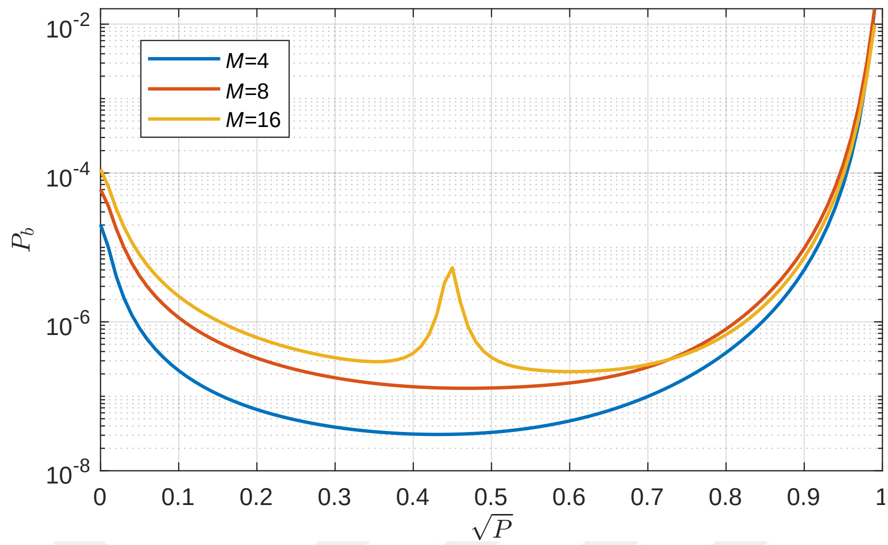

Figure 4.3: Optimum $\sqrt{P}$ search for $n = 2$, varying M, and a fixed SNR of 40 dB.

can be given as in [Basar et al., 2013a]:

$$\begin{aligned} \mathrm{P}(\mathbf{Z} \to \hat{\mathbf{Z}}) &= E_{\mathbf{h}_g}\{\mathrm{P}(\mathbf{Z} \to \hat{\mathbf{Z}}|\mathbf{h}_g)\} \\ &\approx \frac{1/12}{\det(\mathbf{I}_n + \lambda_1 \mathbf{A})} + \frac{1/4}{\det(\mathbf{I}_n + \lambda_2 \mathbf{A})}, \end{aligned} \tag{4.7}$$

where $\lambda_1 = 1/(4N_0)$ and $\lambda_2 = 1/(3N_0)$. Finally, the ABEP of OFDM-PIM can be upper bounded by

$$\mathrm{P}_b \leq \frac{1}{p2^p} \sum_{\mathbf{Z}} \sum_{\hat{\mathbf{Z}}} \mathrm{P}(\mathbf{Z} \to \hat{\mathbf{Z}}) e(\mathbf{Z}, \hat{\mathbf{Z}}), \tag{4.8}$$

where $e(\mathbf{Z}, \hat{\mathbf{Z}})$ is the number of faulty bits for the corresponding error event.

4.4 Power Level Selection Strategy

Let $P_1 = 2 - P$, $P_2 = P$, $2 - P > P$ and $1 > P \geq 0$. Therefore, we have only one variable for power level. Note that $\mathbf{Z}$ and P_b are functions of P. In this section, we find the minimum P_b by searching $\sqrt{P}$ values from 0 to 0.99 with increments 0.01. As seen from Figure 4.3, the optimum value of $\sqrt{P}$ is obtained as 0.43, 0.47, and 0.6 for $M = 4$, 8, and 16, respectively, with the given parameter $n = 2$ for a fixed SNR of 40 dB. When $P = 0$, it becomes a specific case of OFDM-PIM and equivalent to

OFDM-IM with $k = n/2$. When $P = 1$, OFDM-PIM based schemes cannot operate since subcarrier indices become indistinguisable.

4.5 Diversity Order

To prove the diversity order of OFDM-PIM, we investigate the following two cases:

1. Erroneous detection of index bits.

2. Erroneous detection of a single or multiple data symbols when index bits are decoded correctly.

For the first case, due to the inherent feature of IM, $r \geq 2$ is always obtained, where $r = \text{rank}(\mathbf{A})$ determines the diversity order of the system. For example, with $n = 4$, assume that $\mathbf{i} = [1, 3]$ is chosen, however; $\hat{\mathbf{i}} = [2, 3]$ is erroneously decoded. This is the worst case error event since $\mathbf{i}$ and $\hat{\mathbf{i}}$ overlap. We have $r = 2$ even in this error event as in classical OFDM-IM [Basar et al., 2013a]. For the second case, we investigate the following example. For the given parameters $n = 4$, $M = 2$, and $P = 0.073$, assume that $\mathbf{Z}$ with $\mathbf{i} = [3, 4]$, $\mathbf{k} = [1, 2]$ and $\mathbf{x} = [-1, -1]$, is transmitted, neverthless; $\hat{\mathbf{Z}}$ with $\hat{\mathbf{i}} = [3, 4]$, $\hat{\mathbf{k}} = [1, 2]$ and $\hat{\mathbf{x}} = [-1, 1]$, is erroneously decoded. In this case, we have:

$$\mathbf{A} = \begin{bmatrix} 0 & 0 & 0 & 0 \\ 0 & 0.2916 & 0 & 0 \\ 0 & 0 & 0 & 0 \\ 0 & 0 & 0 & 7.7084 \end{bmatrix}, \tag{4.9}$$

thus, we obtain $r = 2$. As in RC-OFDM, the distribution of the data symbols over multiple subcarriers provides diversity order of 2 even for a single symbol decoding error. It can be deduced that we always obtain $r \geq 2$ for all error events of this type. Consequently, according to the discussion above, we have

$$\min_{\mathbf{Z}, \hat{\mathbf{Z}}} \text{rank}(\mathbf{A}) = 2, \tag{4.10}$$

which shows that OFDM-PIM provides a diversity order of 2. OFDM-I/Q-PIM also provides the same diversity order in a similar manner.

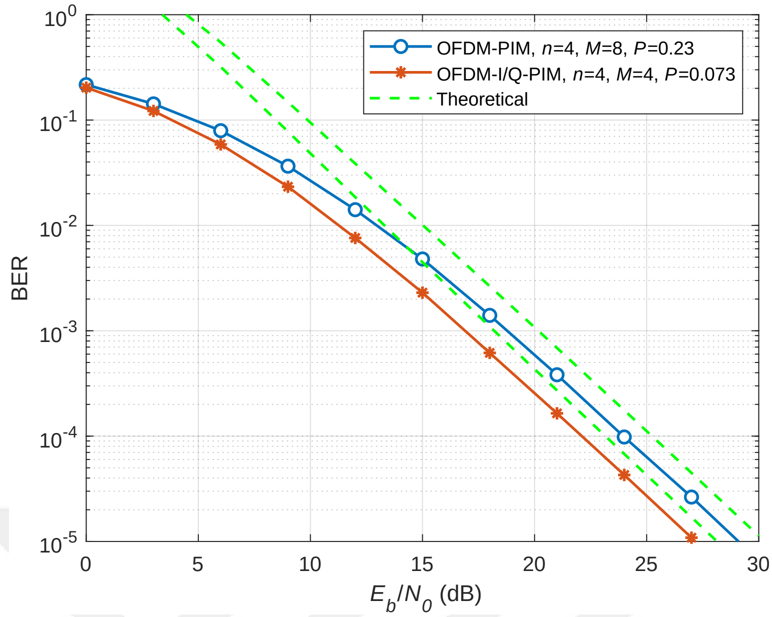

Figure 4.4: Theoretical BER upper bound of OFDM-PIM and OFDM-I/Q-PIM with simulation results for 2 bps/Hz.

4.6 Simulation Results

In this section, we present computer simulation results to compare the error performance of OFDM-PIM and OFDM-I/Q-PIM with OFDM, RC-OFDM, and various OFDM-IM based schemes. The system parameters are considered as: $N = 128$, $T = 10$, and $C = 16$. For OFDM-PIM and OFDM-I/Q-PIM, the optimum P is obtained by the power level selection strategy discussed previously for a fixed SNR value of 40 dB. As seen from Figure 4.4, theoretical curves obtained by (9) behave as upper bounds for OFDM-PIM and OFDM-I/Q-PIM. Moreover, OFDM-I/Q-PIM provides a 2 dB gain over OFDM-PIM at a bit error rate (BER) value of 10^{-5} due to lower order modulation.

In Figure 4.5, the error performance of OFDM-PIM and OFDM-I/Q-PIM is compared with classical OFDM, OFDM-IM, CI-OFDM-IM, OFDM-I/Q/IM, and RC-OFDM. The repetition rate of RC-OFDM is equal to $n = 4$. As seen from Figure 4.5, OFDM-PIM and OFDM-I/Q-PIM provide remarkably better error performance than other schemes. At a BER value of 10^{-5}, OFDM-PIM provides nearly the same error performance with RC-OFDM, however; OFDM-I/Q-PIM achieves a 2 dB gain

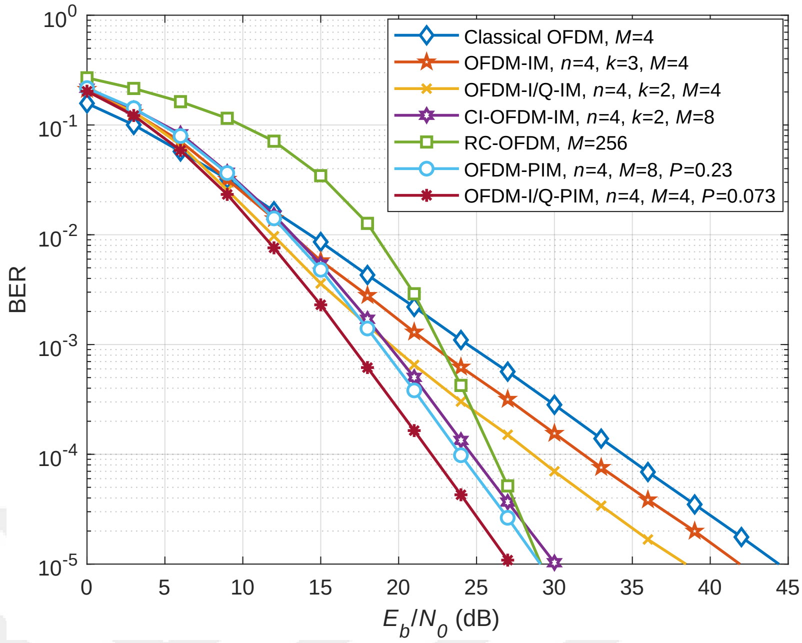

Figure 4.5: Error performance comparison of OFDM-PIM and OFDM-I/Q-PIM with OFDM, RC-OFDM, and CI-OFDM-IM for 2 bps/Hz.

over RC-OFDM. As spectral efficiency increases, RC-OFDM requires a very high modulation order, therefore; the error performance difference between OFDM-PIM-based schemes and RC-OFDM further increases.

Figure 4.6 shows the error performance of OFDM, OFDM-PIM, and OFDM-I/Q-PIM with and without 1/3 rate LTE CC [Ahmadi, 2014]. At a BER value of 10^{-5}, OFDM-PIM and OFDM-I/Q-PIM achieve approximately a 15 dB and 17 dB gain over uncoded-OFDM, respectively. In addition, in the presence of coding, OFDM-PIM and OFDM-I/Q-PIM achieve almost a 2 dB and 3 dB gain over OFDM, respectively. Due to their outstanding error performance, OFDM-PIM-based schemes with coding can be seen as competitive rivals to coded-OFDM which is used in many standards such as IEEE 802.11x.

In Figure 4.7, we compare the error performance of OFDM-PIM to RC-OFDM for varying spectral efficiencies. The repetition rate of RC-OFDM is equal to $n = 2$. As seen from Figure 4.7, the error performance difference betweeen OFDM-PIM and RC-OFDM increases with increasing spectral efficiency. Moreover, OFDM-PIM can achieve significantly high spectral efficiency rates with acceptable SNR values.

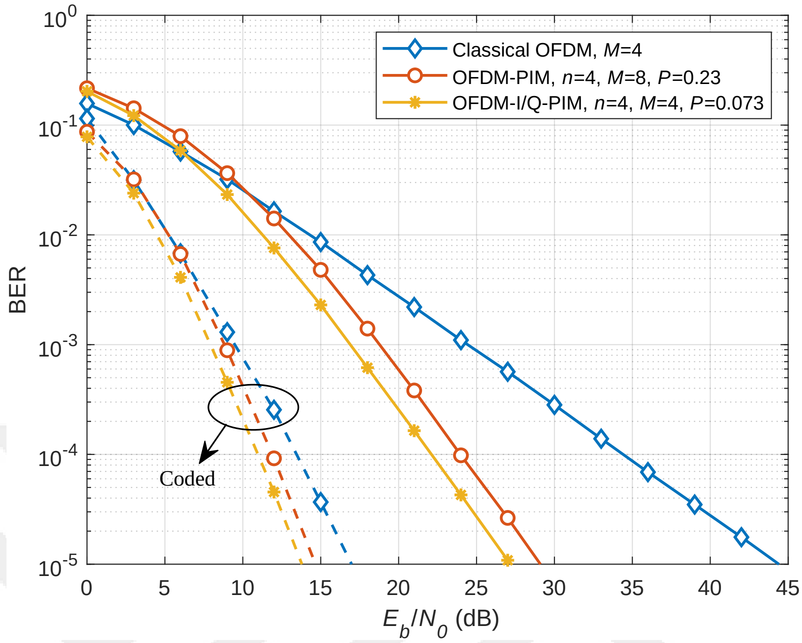

Figure 4.6: Uncoded/Coded error performance comparison of OFDM-PIM and OFDM-I/Q-PIM with OFDM.

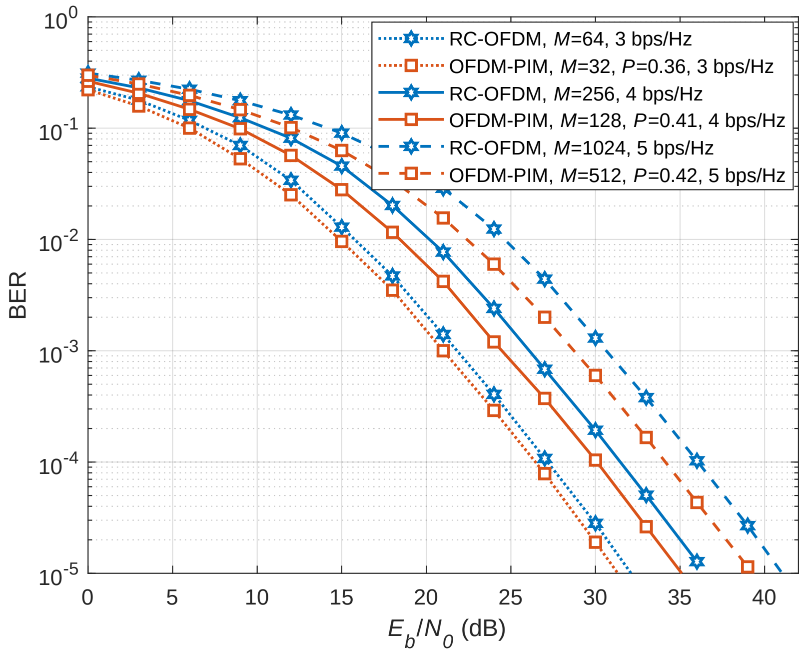

Figure 4.7: Error performance comparison of OFDM-PIM with RC-OFDM for 3, 4, and 5 bps/Hz when $n = 2$.

Chapter 5

ENHANCED SPARSE VECTOR CODING OFDM

In SVC-OFDM, SVC is applied to OFDM-IM by activating only a few number of subcarriers to meet the requirements of URLLC applications. Nonetheless, the number of APs is not always the integer power of two and as a result, all possible APs cannot be utilized. Hence, illegal APs might be detected at the receiver and an effective communication cannot be achieved by erroneously decoding these APs.

In this chapter, E-SVC-OFDM, which is capable of using all possible APs in a clever manner for data transmission, is proposed. In addition to providing reliability and low complexity, E-SVC-OFDM offers higher spectral efficiency compared to plain SVC-OFDM due to the use of all APs. The system model, complexity analysis, and simulation results of E-SVC-OFDM are given in the following sections.

5.1 E-SVC-OFDM Encoder

The block diagram of the considered E-SVC-OFDM system is shown in Figure 5.1. Firstly, using the combinatorial method [Basar et al., 2013a], a sparse vector $\mathbf{s} \in \mathbb{C}^{M\times 1}$, which has K non-zero elements with indices $(i_1, i_2, \cdots, i_K)$, where $i_k \in \{1, \cdots, M\}$ is the kth index, is constructed in the virtual digital domain (VDD)[Zhang et al., 2016] according to the decimal equivalent (d) of the incoming m bits via binary to decimal conversion. Once $(i_1, i_2, \cdots, i_K)$ are selected, K constant unit-energy symbols that do not convey information, are assigned to these active indices similar to space shift keying (SSK) schemes [Basar *et al.*, 2017], where the vector of these symbols is $\mathbf{b}_1 = [x_1, x_2, \cdots, x_K]^{\mathrm{T}}$ and $[.]^{\mathrm{T}}$ denotes the transpose. A total of $\binom{M}{K}$ APs, which can be generated by the combinatorial method and takes d as an input, are available, where $\binom{\cdot}{\cdot}$ is the binomial coefficient. However, only $2^{\lfloor a \rfloor}$ APs can be used, which results in a waste of potential use of all APs, where

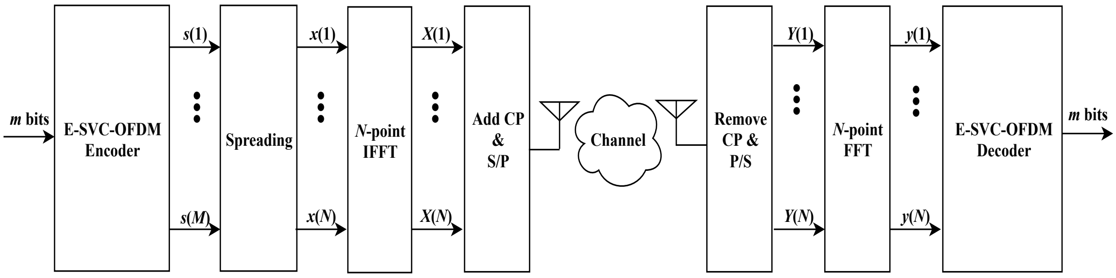

Figure 5.1: System model of E-SVC-OFDM.

$a = \log_2 \binom{M}{K}$ and $\lfloor . \rfloor$ is the floor function. At this point, a clever technique that reuses the remaining $2^{\lfloor a \rfloor + 1} - \binom{M}{K}$ APs by extending the set of constant symbols as $\mathbf{b}_2 = [\tilde{x}_1, \tilde{x}_2, \cdots, \tilde{x}_K]^{\mathrm{T}}$, is proposed. Therefore, a total of $m = \lfloor a \rfloor + 1$ bits can be transmitted for each OFDM symbol. This technique enables us to use all possible APs and to transmit one additional bit. If d is greater than $\binom{M}{K} - 1$, the indices corresponding to $d - \binom{M}{K}$ are reused by extending the constant symbol set. We also avoid illegal APs in this way.

As an example, assume two constant and unit-energy symbols $x_1 = 1$ and $x_2 = j$ are transmitted via active indices for $M = 4$ and $K = 2$. All possible APs can be exploited with the reuse of the first two APs by extending the set of the constant symbols by $\tilde{x}_1 = -1$ and $\tilde{x}_2 = -j$ as shown in Table 5.1. In the absence of this extension, we have a total of 6 APs and only $2^{\lfloor \log_2 6 \rfloor} = 4$ out of them can be employed to convey information. Here, the remaining 2 APs are illegal. As seen from Table 5.1, our proposed method enables the use of all possible APs and the transmission of $\log_2 8 = 3$ bits.

After the formation of $\mathbf{s}$ as above, it is then spread by multiplication with a predefined codebook matrix $\mathbf{C} \in \mathbb{C}^{N \times M}$ whose elements are randomly generated and Bernoulli distributed to enable compressed sensing (CS)-based detection at the receiver [Ji et al., 2018]. After spreading $\mathbf{s}$, the transmitted OFDM block $\mathbf{x}_F \in \mathbb{C}^{N \times 1}$, whose all subcarriers are non-zero, is obtained as:

$$\mathbf{x}_F = [x(1), x(2), \cdots, x(N)]^{\mathrm{T}} = \mathbf{C}\mathbf{s}. \tag{5.1}$$

After this point, the same procedures for OFDM are applied. The IFFT is

Table 5.1: Index combinations according to incoming bits

Bits	d	First Index (i_1)	Second Index (i_2)	First Symbol	Second Symbol
[000]	0	1	2	1	j
[001]	1	1	3	1	j
[010]	2	2	3	1	j
[011]	3	1	4	1	j
[100]	4	2	4	1	j
[101]	5	3	4	1	j
[110]	6	1	2	-1	$-j$
[111]	7	1	3	-1	$-j$

applied to the OFDM block to obtain to the time domain OFDM block $\mathbf{x}_T$:

$$\mathbf{x}_T = \text{IFFT}\{\mathbf{x}_F\} = [X(1), X(2), \cdots, X(N)]^{\text{T}}. \tag{5.2}$$

After the IFFT operation, a CP of length L samples $[X(N-L+1), \cdots, X(N-1)X(N)]^{\text{T}}$ is added to the beginning of the OFDM block. Once parallel to serial (P/S) and digital/analog conversions are applied, the signal is transmitted over a frequency-selective Rayleigh fading channel, which can be represented by the CIR coefficients

$$\mathbf{h}_T = [h_T(1), \cdots, h_T(v)]^{\text{T}}, \tag{5.3}$$

where $h_T(\alpha), \alpha = 1, \ldots, v$ are circularly symmetric complex Gaussian random variables with the $\mathcal{CN}(0, \frac{1}{v})$ distribution. With the assumption that the channel remains constant during transmission of an OFDM block and the CP length L is larger than v, the equivalent frequency domain input-output relationship of this OFDM scheme is given by

$$y_F(\beta) = x_F(\beta)h_F(\beta) + w_F(\beta), \;\; \beta = 1, \ldots, N \tag{5.4}$$

where $y_F(\beta)$, $h_F(\beta)$ and $w_F(\beta)$ are the received signals, the channel fading coefficients and the noise samples in the frequency domain, whose vector forms are given as $\mathbf{y}_F$, $\mathbf{h}_F$ and $\mathbf{w}_F$, respectively. The distributions of $h_F(\beta)$ and $w_F(\beta)$ are $\mathcal{CN}(0, 1)$

and $\mathcal{CN}(0, N_0)$, respectively, where N_0 is the noise variance in the frequency domain, which is equal to the noise variance in the time domain. The SNR is defined as E_b/N_0, where $E_b = (N + L)/m$ is the average transmitted energy per bit. The spectral efficiency of the proposed scheme is

$$\eta = m/(N + L) \text{ [bits/s/Hz]}. \tag{5.5}$$

5.2 E-SVC-OFDM Decoder

At the receiver side, after removing CP and performing FFT, the MMP-DF algorithm [Kwon et al., 2014], whose inputs are given in Table 5.2, is performed to decode $\mathbf{y}_F$ under the assumption of perfect channel state information. MMP-DF is chosen as the algorithm used due to its precise sparse vector recovery and controllable complexity based on the number of candidates desired for approximation. The MMP-DF algorithm outputs a sparse vector $\hat{\mathbf{s}} \in \mathbb{C}^{M\times 1}$ and works by using a tree search with the help of a greedy search method. As long as the performance gain is high at low tree sizes, then the usage of MMP is well-justified [Kwon et al., 2014]. K is fixed to two for efficient operation of the algorithm as in [Ji et al., 2018]. To be able to apply the MMP-DF algorithm, $\mathbf{y}_F$ and $\mathbf{h}_F$ are modified and used as an inputs for the algorithm. The modified received vector can be expressed as[Ji et al., 2018]

$$\hat{\mathbf{y}}_F = \text{diag}(\hat{\mathbf{h}}_F)\mathbf{y}_F, \tag{5.6}$$

where diag$(\cdot)$ creates a diagonal matrix from a vector, $\hat{\mathbf{h}}_F = [e^{j\angle h_F(1)}, \cdots, e^{j\angle h_F(N)}]^{\mathrm{T}}$ and $\angle h_F(\beta)$ is the angle of $h_F(\beta)$. The sensing matrix can be expressed as

$$\mathbf{\Psi} = \text{diag}(\hat{\mathbf{h}}_F \odot \mathbf{h}_F)\mathbf{C}, \tag{5.7}$$

where $\odot$ stands for element-wise multiplication. Other inputs are the numbers of active subcarriers K, number of search expansions Ω, stop threshold value λ and maximum iterations Υ. With all these inputs, MMP-DF algorithm is run and outputs $\hat{\mathbf{s}}$ that only includes K non-zero elements [Kwon et al., 2014].

The AP indices $(\hat{i}_1, \hat{i}_2, \cdots, \hat{i}_K)$, which are obtained from $\hat{\mathbf{s}}$, are applied to the combinatorial algorithm [Basar et al., 2013b] to obtain the decimal number $\hat{d}$. If

Table 5.2: MMP-DF Inputs and Parameters

Inputs	Notation
Modified received vector	$\hat{\mathbf{y}}_F$
Sensing matrix	$\boldsymbol{\Psi}$
Number of active subcarriers	K
Number of search expansions	Ω
Stop threshold	Λ
Maximum iterations	Υ

$2^{\lfloor a \rfloor+1} - \binom{M}{K} \leq \hat{d}$, meaning $(\hat{i}_1, \hat{i}_2, \cdots, \hat{i}_K)$ are non-reused indices, $\hat{d}$ can be directly converted to bits. Otherwise, the two vectors $\mathbf{b}_1$ and $\mathbf{b}_2$ that contain the symbols $(x_1, x_2, \cdots, x_K)$ and the extended ones $(\tilde{x}_1, \tilde{x}_2, \cdots, \tilde{x}_K)$, respectively, are used for detection. For this purpose, the vector $\hat{\mathbf{b}} = \begin{bmatrix} \hat{b}_1 & \hat{b}_2 & \cdots & \hat{b}_K \end{bmatrix}^{\mathrm{T}}$, which includes the non-zero elements of $\hat{\mathbf{s}}$, is constructed. Finally, in the following, two decision metrics are calculated to find whether the original symbols or extended ones are employed:

$$\hat{l} = \arg\min_{l \in 1,2} \|\hat{\mathbf{b}} - \mathbf{b}_l\|^2. \tag{5.8}$$

If $\hat{l} = 1$, corresponding to the original symbols, then $\hat{d}$ is directly converted to bits. On the other hand, if $\hat{l} = 2$, which represents the extended symbols, $\hat{d} + \binom{M}{K}$ is converted to bits. To further illustrate the E-SVC-OFDM decoder, a simple example is shown in Figure 5.2.

5.3 *Complexity Analysis*

In this section, we analyze the complexity of E-SVC-OFDM detectors in terms of the running time as in [Kwon et al., 2014]. The MATLAB software on a computer with an Intel Core i7-3930K processor and Microsoft Windows 10 environment have been exploited to obtain the running time. In [Kwon et al., 2014], it is stated that MMP-DF algorithm is comparable with other greedy algorithms such as StOMP [Donoho et al., 2012] and CoSaMP [Needell and Tropp, 2010] when K is low. In our proposed schemes, $K = 2$ have been selected, therefore, the employed algorithm can be considered as a low-complexity one. Also, since channel coding is not required

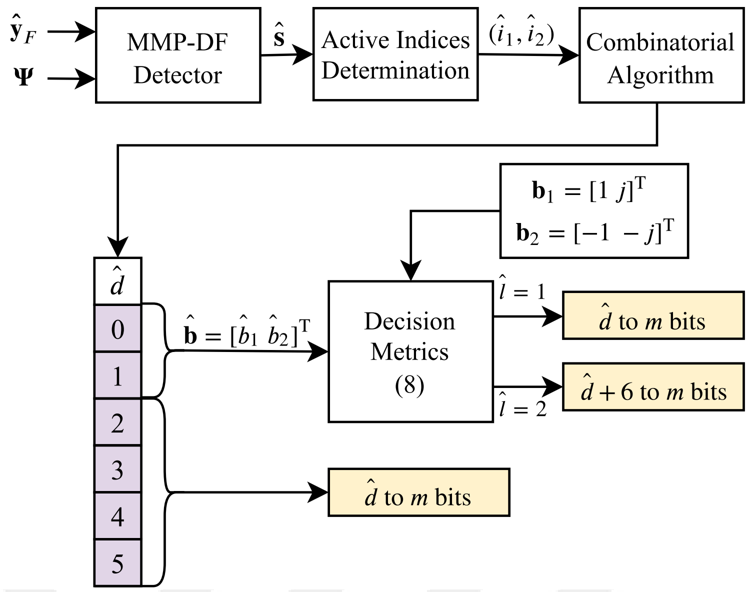

Figure 5.2: A flow diagram example of the E-SVC-OFDM decoder for $M = 4$ and $K = 2$.

to achieve outstanding BER in E-SVC-OFDM, it is relatively a much less complex scheme when compared to channel coded ones. To give further insight into the decoding complexity, it is showed that the comparison of ML detection and the proposed detectors in Figure 5.3. Assume that the set including all possible sparse vectors in VDD is given by $\mathcal{X} = \{\mathbf{x}_1, \cdots, \mathbf{x}_{2^{\lfloor a \rfloor + 1}}\}$. Then, by employing $\mathcal{X}$, ML detection rule for E-SVC-OFDM can be obtained as:

$$\hat{\mathbf{x}} = \arg\min_{\mathbf{x}\in\mathcal{X}} \|\mathbf{y}_F - \mathbf{h}_F \odot (\mathbf{C}\mathbf{x})\|^2. \tag{5.9}$$

As seen from Figure 5.3, ML detection is inefficient in terms of complexity for the proposed schemes. However, MMP-DF algorithm presents much lower complexity compared to ML method. In Figure 5.3, since K is low, the MMP-DF detector is more efficient than the ML detector as in [Kwon et al., 2014]. It should be noted that the complexity of the decision metric calculations in (5.9) after the MMP-DF algorithm to determine whether the symbols are extended, is negligible and can be ignored. Additionally, in contrast to ML detection, MMP-DF is not effected by M since K is constant.

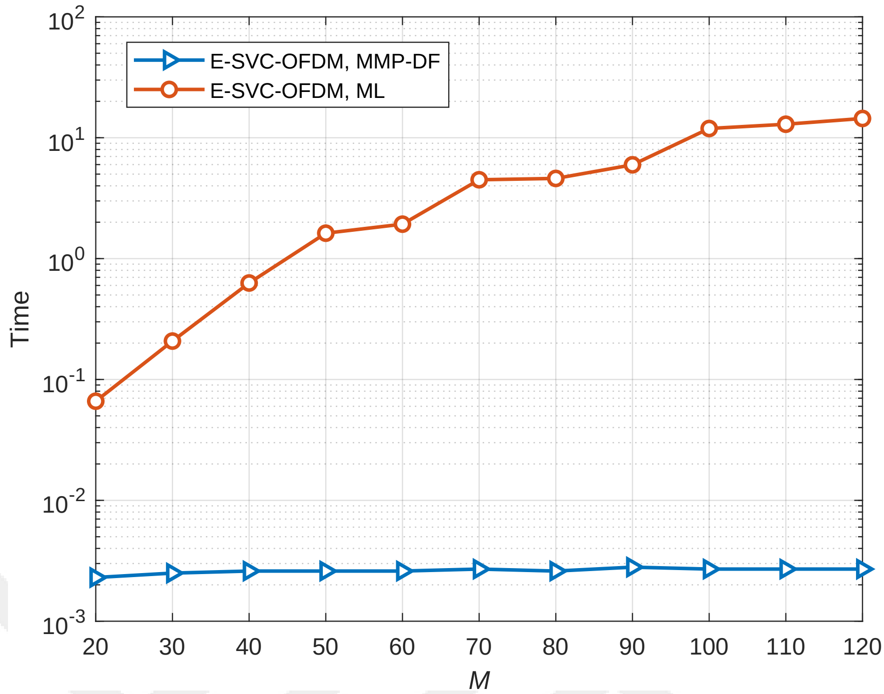

Figure 5.3: Running time as a function of M where the proposed scheme use ML and MMP-DF detection.

5.4 Simulation Results

In this section, computer simulation results are presented for varying parameters of E-SVC-OFDM. Additionally, a BER comparison is shown for convolutional coded OFDM [Ahmadi, 2014] and E-SVC-OFDM. Error performance of these schemes are obtained through Monte Carlo simulations. For all simulations, a 10-tap frequency-selective Rayleigh fading channel and two active indices ($K = 2$) in the VDD is assumed, where $x_1 = 1$, $x_2 = j$ and $\tilde{x}_1 = -1$, $\tilde{x}_2 = -j$. The CP length is set as 16 and the LTE CC with rate 1/3 was chosen [Ahmadi, 2014]. The parameters Ω, Λ and Υ for the MMP-DF algorithm are set as 2, 0.1, and 2, respectively.

The first simulation involves only the E-SVC-OFDM scheme with a varying number of subcarriers (N) in the frequency domain as $M = 128$ is kept constant, which changes the spectral efficiency. As seen from Figure 5.4a, as the number of elements in the virtual domain is kept constant and the number of subcarriers are escalated from 32 to 512, a noticeable improvement is observed in BER performance due to

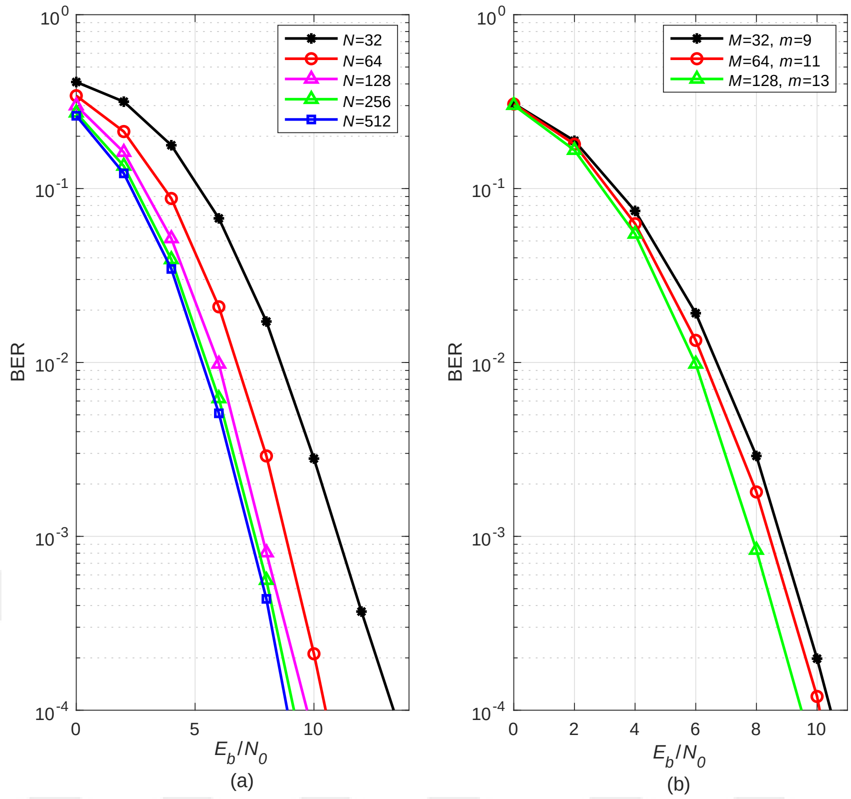

Figure 5.4: Error performance of E-SVC-OFDM (a) for $M = 128$ and varying N and (b) for $N = 128$ and varying M.

the APs of the sparse vector being spread to more resources in the frequency domain. In other words, spreading the APs to more subcarriers provides a coding gain. As N increases, the correlation between randomly generated codewords decreases, and this helps with better recovery of sparse vectors. However, spectral efficiency decreases as the number of subcarriers increases because more spectrum is used with more subcarriers. It is also seen in Figure 5.4a that the BER improvement reaches a saturation while the largest improvement occurs until $N \leq M$.

In Figure 5.4b, the number of subcarriers is fixed to 128, and the number of elements in the virtual domain (M) is varied as $32, 64$ and 128. It is observed that with increasing the size of the virtual domain, the error performance improves relatively. This can be explained by the fact that as M increases, sparsity increases resulting in an improvement in BER and an increase in the number of transmitted bits.

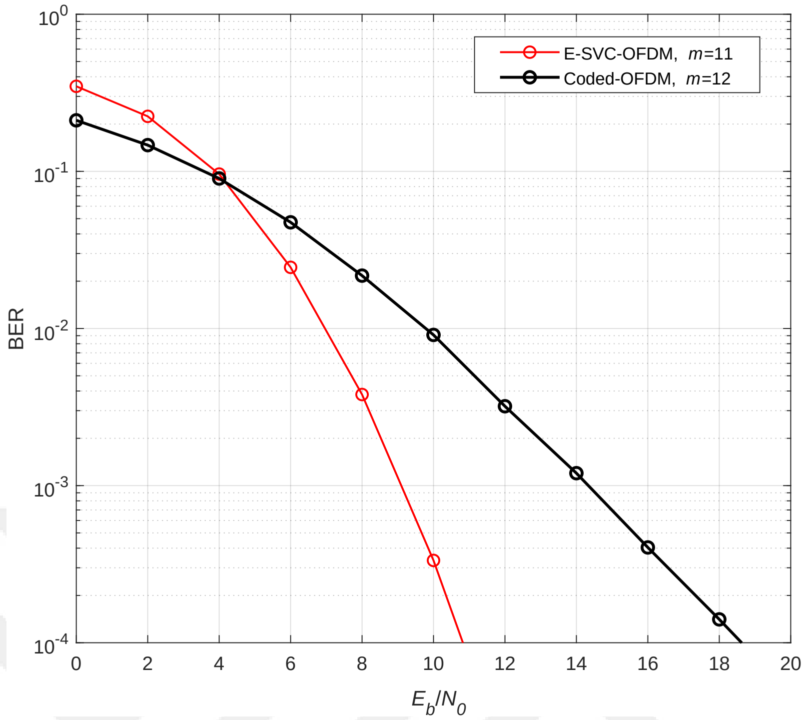

Figure 5.5: Error performance of E-SVC-OFDM and Coded-OFDM for $N = 64$ and $M = 64$.

Finally, the proposed scheme is compared to the existing LTE convolutional coded OFDM [Ahmadi, 2014] with zero padding in Figure 5.5. Zero padding has been used for coded OFDM to obtain the same spectral efficiency with the proposed scheme and employed random interleaving to improve its performance. E-SVC-OFDM provides an outstanding BER with an improvement of 8 dB compared to coded-OFDM and relatively lower complexity due to the requirement of coding being removed.

Chapter 6

CONCLUSION

In this thesis, three novel OFDM-based waveforms are proposed for two different 5G services: eMBB and URLLC.

First, SuM-OFDM-IM, which jointly determines MAPs and SAPs by IM to convey additional information bits and replicates the conventional QAM/PSK symbols to obtain a diversity gain, have been proposed. Furthermore, the separate selection of MAPs and SAPs has also been investigated. A reduced complexity ML detector, which achieves the same error performance as the ML detector, has been designed and its complexity analysis has been given. Finally, the error performance of the proposed scheme has been investigated both with computer simulations and SDR modules under practical impairments. Exhaustive simulation and practical results demonstrate that the proposed scheme remarkably outperforms OFDM and other OFDM-IM based reference systems in terms of error performance while providing a high spectral efficiency. Consequently, SuM-OFDM-IM can be a possible waveform candidate for 5G and beyond eMBB services due to its appealing advantages such as high spectral efficiency, reliability and diversity gain.

Secondly, a novel OFDM-IM based scheme have been proposed called OFDM-PIM. In OFDM-PIM, the error performance is enhanced by applying power distribution to the subcarrier indices of conventional OFDM-IM. OFDM-I/Q-PIM is proposed by extending OFDM-PIM to in-phase and quadrature dimensions to further increase the number of index bits transmitted. OFDM-PIM based schemes can be considered as potential waveforms for 5G and beyond wireless communication systems due to their superior features such as remarkable error performance, simple and flexible transciever structure, diversity gain, and high spectral efficiencies.

Lastly, E-SVC-OFDM scheme have been presented as reliable and low-latency waveform. E-SVC-OFDM provides a clever and efficient use of the APs compared to the existing SVC-OFDM. The improved BER of the E-SVC-OFDM scheme over the existing coded-OFDM scheme has been demonstrated through Monte Carlo simulations.

Consequently, SuM-OFDM-IM can be a possible waveform candidate for 5G and beyond eMBB services due to its appealing advantages such as high spectral efficiency, reliability and diversity gain. Other precoding techniques can be employed to further increase the diversity order of SuM-OFDM-IM. Moreover, the spectral efficiency can be further enhanced by selecting more than two modes; however, this is beyond the scope of this thesis and will be considered in our future studies. OFDM-PIM based schemes can also be considered as potential waveforms for 5G and beyond wireless communication systems due to their superior features such as remarkable error performance, simple and flexible transciever structure, diversity gain, and high spectral efficiencies. The practical implementation of OFDM-PIM and OFDM-I/Q-PIM by employing software defined radios (SDRs) is planned as a future study. E-SVC-OFDM provides remarkable error performance and very low complex decoding. Further reliability and latency improvements with generalized designs may be possible and left as future work. We hope that this thesis might be useful for researchers working towards waveform design for next-generation wireless networks.

BIBLIOGRAPHY

[Ahmadi, 2014] Ahmadi, S. (2014). LTE-advanced: A practical systems approach to understanding 3GPP LTE releases 10 and 11 radio access technologies. *LTE-Advanced: A Practical Systems Approach to Understanding 3GPP LTE Releases 10 and 11 Radio Access Technologies*, pages 1–1116.

[Arslan and Reddy, 2003] Arslan, H. and Reddy, S. (2003). Noise power and SNR estimation for OFDM based wireless communication systems. In *Proc. of 3rd IASTED Int. Conf. on Wireless Optical Commun. (WOC), Banff, Alberta, Canada.*

[Başar and Panayırcı, 2015] Başar, E. and Panayırcı, E. (2015). Optical OFDM with index modulation for visible light communications. In *2015 4th International Workshop on Optical Wireless Communications (IWOW)*, pages 11–15.

[Basar, 2015] Basar, E. (2015). OFDM with index modulation using coordinate interleaving. *IEEE Wireless Commun. Lett.*, 4(4):381–384.

[Basar, 2016a] Basar, E. (2016a). Index modulation techniques for 5G wireless networks. *IEEE Commun. Mag.*, 54(7):168–175.

[Basar, 2016b] Basar, E. (2016b). On multiple-input multiple-output OFDM with index modulation for next generation wireless networks. *IEEE Trans. Signal Process.*, 64(15):3868–3878.

[Basar et al., 2013a] Basar, E., Aygölü, Ü., Panayırcı, E., and Poor, H. V. (2013a). Orthogonal frequency division multiplexing with index modulation. *IEEE Trans. Signal Process.*, 61(22):5536–5549.

[Basar et al., 2013b] Basar, E., Aygolu, U., Panayırcı, E., and Poor, H. V. (2013b). Orthogonal frequency division multiplexing with index modulation. *IEEE Trans. Signal Process.*, 61(22):5536–5549.

[Basar et al., 2017] Basar, E., Wen, M., Mesleh, R., Di Renzo, M., Xiao, Y., and Haas, H. (2017). Index modulation techniques for next-generation wireless networks. *IEEE Access*, 5:16693–16746.

[Basar *et al.*, 2017] Basar *et al.*, E. (2017). Index modulation techniques for next-generation wireless networks. *IEEE Access*, 5:16693–16746.

[Cho et al., 2010] Cho, Y. S., Kim, J., Yang, W. Y., and Kang, C. G. (2010). *MIMO-OFDM Wireless communications with MATLAB*. John Wiley & Sons.

[CoreLab, 2020] CoreLab (2020). Communications research and innovation laboratory. `http://corelab.ku.edu.tr`.

[Dang et al., 2018a] Dang, S., Chen, G., and Coon, J. P. (2018a). Outage performance of two-hop OFDM with index modulation and multi-carrier relay selections. *IEEE Wireless Commun. Lett.*, 7(6):926–929.

[Dang et al., 2018b] Dang, S., Coon, J. P., and Chen, G. (2018b). Adaptive OFDM with index modulation for two-hop relay-assisted networks. *IEEE Trans. Wireless Commun.*, 17(3):1923–1936.

[Donoho et al., 2012] Donoho, D. L., Tsaig, Y., Drori, I., and Starck, J. (2012). Sparse solution of underdetermined systems of linear equations by stagewise orthogonal matching pursuit. *IEEE Trans. Inf. Theory*, 58(2):1094–1121.

[Gokceli et al., 2017] Gokceli, S., Basar, E., Wen, M., and Kurt, G. K. (2017). Practical implementation of index modulation-based waveforms. *IEEE Access*, 5:25463–25473.

[Jaradat et al., 2018] Jaradat, A. M., Hamamreh, J. M., and Arslan, H. (2018). OFDM with subcarrier number modulation. *IEEE Wireless Commun. Lett.*, 7(6):914–917.

[Ji et al., 2018] Ji, H., Park, S., and Shim, B. (2018). Sparse vector coding for ultra reliable and low latency communications. *IEEE Trans. Wireless Commun.*, 17(10):6693–6706.

[Kwon et al., 2014] Kwon, S., Wang, J., and Shim, B. (2014). Multipath matching pursuit. *IEEE Trans. Inf. Theory*, 60(5):2986–3001.

[Li et al., 2018] Li, Q., Wen, M., Basar, E., Poor, H. V., Zheng, B., and Chen, F. (2018). Diversity enhancing multiple-mode OFDM with index modulation. *IEEE Trans. Commun.*, 66(8):3653–3666.

[Li et al., 2019] Li, Q., Wen, M., Dang, S., Basar, E., Poor, H. V., and Chen, F. (2019). Opportunistic spectrum sharing based on OFDM with index modulation. *IEEE Trans. Wireless Commun.*, pages 1–1.

[Lu et al., 2018] Lu, S., Hemadeh, I. A., El-Hajjar, M., and Hanzo, L. (2018). Compressed-sensing-aided space-time frequency index modulation. *IEEE Trans. Veh. Techol.*, 67(7):6259–6271.

[Ma et al., 2017] Ma, Q., Yang, P., Dan, L., He, X., Xiao, Y., and Li, S. (2017). OFDM-IM-aided cooperative relaying protocol for cognitive radio networks. In *2017 IEEE 18th Int. Workshop on Signal Processing Advances in Wireless Commun. (SPAWC)*, pages 1–5.

[Mao et al., 2017a] Mao, T., Wang, Q., and Wang, Z. (2017a). Generalized dual-mode index modulation aided OFDM. *IEEE Commun. Lett.*, 21(4):761–764.

[Mao et al., 2018] Mao, T., Wang, Q., Wang, Z., and Chen, S. (2018). Novel index modulation techniques: A survey. *IEEE Commun. Surveys Tuts*, 21(1):315–348.

[Mao et al., 2017b] Mao, T., Wang, Z., Wang, Q., Chen, S., and Hanzo, L. (2017b). Dual-mode index modulation aided OFDM. *IEEE Access*, 5:50–60.

[Mesleh et al., 2006] Mesleh, R., Haas, H., Ahn, C. W., and Yun, S. (2006). Spatial modulation-a new low complexity spectral efficiency enhancing technique. In *2006 First International Conference on Communications and Networking in China*, pages 1–5. IEEE.

[Moose, 1994] Moose, P. H. (1994). A technique for orthogonal frequency division multiplexing frequency offset correction. *IEEE Trans. Commun.*, 42(10):2908–2914.

[Nambi and Giridhar, 2018] Nambi, S. A. and Giridhar, K. (2018). Lower order modulation aided BER reduction in OFDM with index modulation. *IEEE Commun. Lett.*, 22(8):1596–1599.

[Needell and Tropp, 2010] Needell, D. and Tropp, J. A. (2010). Cosamp: Iterative signal recovery from incomplete and inaccurate samples. *Commun. ACM*, 53(12):93–100.

[Öztürk et al., 2019] Öztürk, E., Basar, E., and Çırpan, H. A. (2019). Multiple-input multiple-output generalized frequency division multiplexing with index modulation. *Physical Communication*, 34:27–37.

[Popovski et al., 2018] Popovski, P., Trillingsgaard, K. F., Simeone, O., and Durisi, G. (2018). 5G wireless network slicing for eMBB, URLLC, and mMTC: A communication-theoretic view. *IEEE Access*, 6:55765–55779.

[Sasamori et al., 2011] Sasamori, F., Jia, Z., Handa, S., and Oshita, S. (2011). Performance analysis of repetition coded OFDM systems with diversity combining and higher-level modulation. *IEICE Trans. Commun.*, 94(1):194–202.

[Shi et al., 2019] Shi, Y., Gao, K., Zhu, J., Lu, X., and Wang, S. (2019). Orthogonal frequency division multiplexing with joint subblocks index modulation. *IEEE Access*, 7:23930–23939.

[Wen et al., 2017] Wen, M., Basar, E., Li, Q., Zheng, B., and Zhang, M. (2017). Multiple-mode orthogonal frequency division multiplexing with index modulation. *IEEE Trans. Commun.*, 65(9):3892–3906.

[Wen et al., 2018] Wen, M., Li, Q., Basar, E., and Zhang, W. (2018). Generalized multiple-mode OFDM with index modulation. *IEEE Trans. Wireless Commun.*, 17(10):6531–6543.

[Xiao et al., 2014] Xiao, Y., Wang, S., Dan, L., Lei, X., Yang, P., and Xiang, W. (2014). OFDM with interleaved subcarrier-index modulation. *IEEE Commun. Lett.*, 18(8):1447–1450.

[Zhang et al., 2016] Zhang, H., Yang, L.-L., and Hanzo, L. (2016). Compressed sensing improves the performance of subcarrier index-modulation-assisted OFDM. *IEEE Access*, 4:7859–7873.

[Zheng et al., 2017] Zheng, B., Wen, M., Basar, E., and Chen, F. (2017). Multiple-input multiple-output OFDM with index modulation: Low-complexity detector design. *IEEE Trans. Signal Process.*, 65(11):2758–2772.

[Zheng and Chen, 2017] Zheng, J. and Chen, R. (2017). Achieving transmit diversity in OFDM-IM by utilizing multiple signal constellations. *IEEE Access*, 5:8978–8988.